Optical Coupling System Optimization for Medical Laser Surgical Applications

Hannah Brooks, Zhuofan Lu, Karina Mirochnik, Olivia Petropulos

Worcester Polytechnic Institute

Major Qualification Project Report

Advisor: Professor Yuxiang Liu
Co-advisor: Professor Loris Fichera
February 1, 2022

Abstract

In this report, we develop and optimize a compact, modular optical coupling system that couples light from an 400-µm-diameter Endostat fiber into a 200-µm-diameter multimode fiber, to enable steering for practical clinical use of endoscopic procedures for laryngeal lesions and other applications. The current commercial laser surgical systems were not able to effectively treat and reach all affected regions of the larynx due to their lack of steerability and efficiency, thus making them underutilized in clinical practices. The efficiency of the system determines how practical it can be during clinical use given the demand of medical needs. There has been a fiber coupling system in the lab from the previous year's students, but the system was large, heavy, and not suitable for the aim of clinical applications. Therefore, we develop an optical fiber free-space coupling system - as a part of a robotic system - that channels light from a thick fiber in a commercial laser surgery system into a thinner multimode fiber to enable endoscope probe steering in confined spaces such as a larynx. Our work began by developing a smaller, portable, and more efficient coupling system through 12 design iterations. Prototypes for these design iterations were fabricated and tested via a power meter to determine the optical transmission efficiency of the system. A maximum efficiency of 53% was reached in the final design iteration. Besides the efficiency, the current system also achieved compactness in terms of the nearly 70% size reduction from the initial setup. After developing the new coupling system, the team progressed to biological testing on pig ears, larynges, and esophagi to determine the efficiency and compatibility of the system with human skin like tissues. The laser was tested on biological samples to determine how much damage can be done over a series of different exposure times. Exposure times tested ranged from 2 to 10 seconds, and the rest of the variables were held constant throughout. The average depth achieved for each exposure time is as follows: 2 seconds caused 461.08 µm of damage, 4 seconds caused 670.92 µm of damage, 6 seconds caused 907.09 µm of damage, 8 seconds cause 1284.26 µm of damage, and 10 seconds caused 1430.95 µm of damage. We found that the depth increases by about 200 µm with every 2 seconds of applied laser light. The depth values allows a clinician to estimate how long they need to hold the laser on a lesion depending on the lesion dimensions. The team also conducted testing on C2C12 cell samples. This study found that 2 seconds of 532 nm wavelength green light from the laser system produced 48.9% cellular detachment from the plate/death, 4 seconds produced 52.8% detachment, 6 second produced 53.3% detachment, 8 seconds produced 64,3% detachment and 10 seconds produced 70.8% detachment. This finding supports the idea that the energy put into the system shares a positive relationship with the damage done to the cells, in addition to demonstrating the capabilities of our coupling system for laser surgical applications. We believe that the efficiency and biological testing conducted in this report strongly support the conclusion that our optical free space coupling system is efficient and effective for coupling light to a customized thin fiber, which enables the surgical laser steering while retaining enough optical power for desired tissue damage, and our work has considerable potential in numerous clinical applications including laser surgeries and endoscopy.

Table of Contents

List of Figures

Chapter 1: Introduction

1.1 Motivation and Needs

Laser therapy is a common medical procedure that uses a strong beam of light to cut, burn, or destroy tissue. The current laser used for these procedures holds limitations in its effectiveness and precision. A laser coupling system can be used to transfer light from a larger diameter optical fiber into a smaller one to allow for more precise procedures. Thinner optic fiber can achieve a smaller bending radius, this smaller bending radius allows for better manipulation of the fiber. The increased manipulation correlates directly to increased precision. Increased precision allows the surgeon to use the system for more complex applications. There are a multitude of procedures and therapies that would benefit from a laser coupling system combined with an endoscope. This includes tonsillectomies, stapedectomies, and acupuncture applications. The best procedures to use this system for are ones that are done in a confined space and utilize an endoscope. One procedure that this system could be applied to is the removal of tumor growths in the larynx.

Benign lesions of the larynx affect an estimated 6.6 % - 7.6 % of adults worldwide, leading to a variety of complications including speech impairment, difficulty in swallowing, and even respiratory obstruction [1]. The current treatment options for laryngeal lesions vary. The anatomical location of these lesions impacts possible treatment options due to the accessibility of different treatment methods. Therefore the use of current non-steerable laser therapy may not be an option if the lesion is not accessible by the surgical fiber. Non-steerable systems come with a decreased ability to manipulate a fiber optic cable to reach difficult places in the larynx. The lack of steering increases the risk of the procedure that the patient must go through, the impact to the patient's quality of life quality during the recovery, and the time and resources that the clinician must spend on the patient for the treatments. The system without the steering mechanism can only treat lesions located along a straight path near the glottis due to its large bending radii [7]. The limited access area of the fiber-delivered laser hinders the application of this procedure. In these cases, doctors opt for more dangerous medical procedures like a cordectomy. Cordectomies are a more invasive procedure, in which the surgeon manually removes the lesions out of the throat. This leads to the removal of part or all of the vocal cords.

An alternative, less invasive approach is an office-based procedure that uses laser pulses to treat larynx lesions endoscopically [3,4]. Laser surgery destroys the blood supply to the lesions while leaving surrounding healthy tissue intact, opposed to comparable non-laser procedures. This is accomplished by targeting the hemoglobin in the blood, a characteristic known as regioselectivity. There is no cutting or excessive bleeding involved, leading to less pain and complications for the patient [9]. This method is favorable because patients do not need general anesthesia and can walk out of the clinic with little impact after five minutes of treatment [2, 5]. For physicians, this endoscopic procedure can be carried out easily in various office environments. The current setup for in-office laser laryngeal treatment is to insert a non-steerable optical fiber through the patient's nose down the throat with visual assistance by a small chip-tip

camera [6]. The steerability, size, and efficiency of the current setup must be improved to allow the physician to effectively reach all parts of the larynx where lesions can occur.

There is an urgent need for a flexible, small diameter steerable fiber inside a flexible endoscope to treat laryngeal lesions. Traditional medical lasers require a larger diameter optical fiber for connection, therefore, smaller diameter fibers cannot be inserted directly into the laser machine. To implement the smaller diameter optical fiber inside a flexible endoscope, a coupling system that can align the laser beam from the larger optical fiber into a smaller one is needed. Therefore, we want to improve the current optical fiber free-space coupling system - as a part of a robotic system - that couples light from a fiber in a commercial laser surgery system into a smaller multimode fiber to enable endoscope probe steering in a confined space with a higher power transmission efficiency and more systematic robustness.The current prototype setup performed the feasibility study and there are still some factors that hinder the practical clinical use including heavyweight, immovable setup, and the time-consuming when performing fine alignment of the system.

The system described above is also a way to meet the need of a greater issue; the need for a system that can eliminate tissue in areas that cannot be reached with existing systems. This idea brings about a multitude of different applications. Some examples of these applications could be the ablation of tonsil tissue in a tonsillectomy. Another example is the use of a laser system to eliminate breast cancer tissue. In order to do any of these procedures, there is a need for a steerable fiber optic cable. Commercial fibers that are used with medical grade lasers are thick and do not have a great range of bending [29]. A greater bending angle can be achieved with a thinner fiber. The hope is to create a system that delivers the surgical laser with a small, flexible, and steerable fiber. Therefore, light from the medical fiber must be translated into a much smaller fiber via the use of light coupling, a topic that will be subsequently discussed. This much larger goal of creating a steerable laser system can be applied to an abundance of medical procedures that require the ablation of benign or malignant cells, beyond laryngeal surgery. Laser pulses to affected regions have the potential to kill lesions and tumors. To prove that a laser coupling system is effective enough to induce damage, analysis of laser damage to tissue and cells can validate the effectiveness of the system for all the proposed applications.

1.2 Background

The main goal of this project was to create a system in which a common medical grade laser with the larger diameter optical fiber can be coupled into a smaller, more versatile fiber for greater medical applications. The laser system must also be efficient enough to achieve cellular damage at a rate that can be quantified. Therefore, our system must include a design that is small, moveable, and easy to align; all with the intention of maximizing the efficiency of commercially available medical lasers. The main components of our system that impact this goal include the optical fibers, collimators, and the medical laser.

We continued the work of previous optical coupling system research completed by Professor Yuxiang Liu et. al. of Worcester Polytechnic Institute in 2020. The existing system available prior to the start of this project was a large, heavy coupling system with low efficiency. This

setup was equipped with alignment in all directions. In addition, it was constructed all from metal, offering a sturdy setup. Moreover, the coupling system achieved with two different collimators did resolve the issue of the bulky endostat fiber being the only point of operation during surgical procedures. With the multimode fiber as the point of patient contact, a smaller fiber with a smaller bending radius was made operational for medical procedures. On the downside, this setup is far too large, not portable, has a low efficiency, and could benefit from some updated components. All of these aspects must be improved prior to effective clinical use.

To make these improvements, it is imperative to understand all the components of the system. All components used in this system can be seen in figure 1 below. The function of each of these components will be discussed further throughout this report.

Collimator #2

Collimator #1

Laserscope KTP/532
Surgical laser

Patient Fiber

Endostat Fiber

Figure 1: Components of the optical fiber free-space coupling system setup

1.2.1 Geometry and Structures of Fiber Optics

The first major structural component of the free-space coupling system is the optical fibers. Optical fibers are, in the most basic sense, "pipes that carry light" [17]. They are hair-thin fibers that are made of ultra-pure drawn glass or plastic, which can carry optical signals like wavelengths from a laser, theoretically to an infinite distance. Light is guided through an optical fiber by the fiber's "core". This core is made of either extremely pure glass or plastic and is surrounded by a second layer of ultra-pure glass or plastic called "cladding". Surrounding the cladding is another layer known as the "buffer". The buffer serves as a protective coating for the fiber to ward off any moisture or physical damage to the fiber [28].
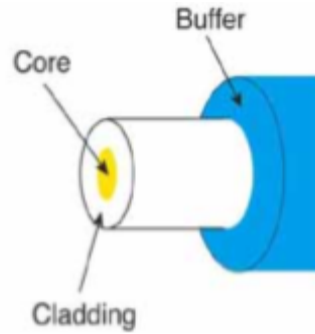
Figure 2: General Optical
Fiber [28]

The free-space coupling system used in this project consists of two different optical fibers, which can be seen in figure 2 above. The first fiber used was a commercially available medical-grade optical fiber that has a large (600 μm), silica core with a polymer coating. This fiber transmits light from the medical laser to the coupling system. The second fiber used has a core diameter of 200 ± 5 μm, a cladding diameter of 225 ± 5 μm, and a 500 ± 30 μm coating diameter [29]. The medical-grade multimode fiber is made of a silica core, polymer coating, and teazel buffer. An image of this makeup can be seen in figure 3. Knowing the design specifications for the optical fibers in use allows the team to employ the most effective optical fiber for the free-space coupling system.
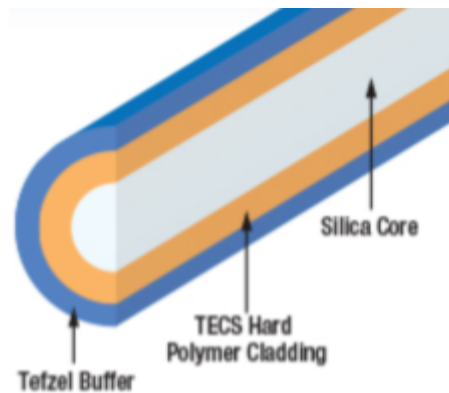
Figure 3: Medical Grade
Multimode Optical Fiber [29]

1.2.2 Light Guiding in Fiber Optics

Transmission of light through these fibers occurs due to an optical technique called "total internal reflection". Total internal reflection occurs because optical fiber cores have a specific known value that quantifies the speed of light through the core. This speed is known as the index of refraction and is what causes light to bend within a medium [28]. Optical fiber cores have a higher index of refraction than their cladding, which causes light to reflect off the surface of the

core. This phenomenon is known as total internal reflection and is what traps light within the core of optical fiber [28].

Due to the versatility and application potential, there are many different types of optical fibers that can be defined as either singlemode or multimode, with varying core/cladding specifications [28]. Single Mode optical fibers generally have a very small core which forces light to travel in only one ray. Conversely, multimode fibers have larger cores that allow light to travel in many rays within the core. The core and cladding of multimode fibers are generally made of different optical materials and reflect light through many different path lengths throughout the core [28].
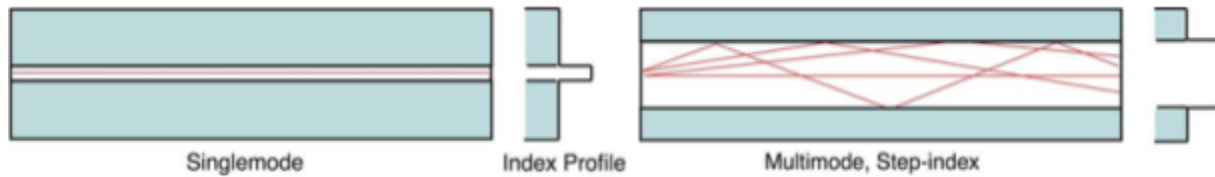
Figure 4: Multimode and Singlemode Fiber [28]

1.2.3 Additional Issues Concerning the Preparation of Fiber Tip

One of the main goals of this project is to increase the efficiency of the laser coupling system, which involves the laser, the fibers, and the collimators, to produce a system that has enough power to damage tissue. To reach our goal of improving efficiency, in addition to knowing the correct design specifications for the optical fiber's purpose, the maintenance and upkeep of the fibers also greatly impact the efficiency of medical laser output. One way to increase the efficiency of the system is to polish the medical fiber as well as the patient output fiber which can be seen in figure 1 above. This is because when an optical fiber is used, very concentrated light at a high wavelength is transmitted through a small area. The small area at the tip of an optical fiber becomes extremely hot due to the concentration and speed of light. This heat melts small particulates that are circulating throughout the air and cause the tip of the optical fiber to char as seen in figure 5a below. When this occurs, the transmission of light through the optical fiber can drastically lose efficiency. Therefore, it is necessary to continuously polish the optical fiber (seen in figure 5b) to ensure the best performance of the system.
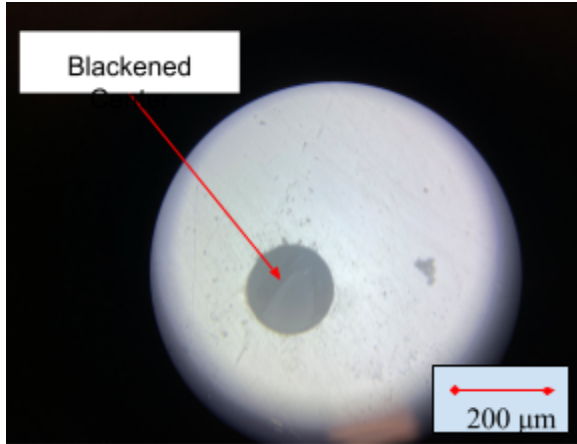
Figure 5a: Completely Burned Optical Fiber
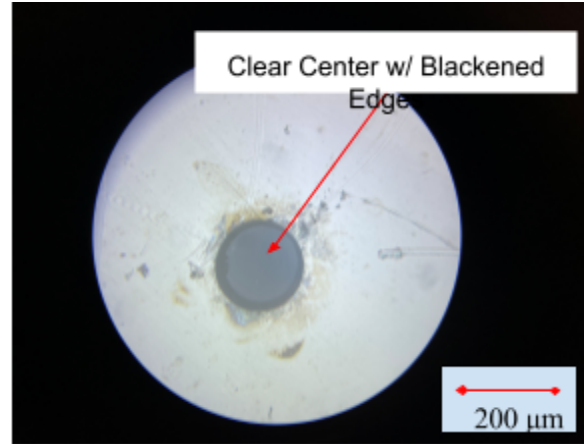
Figure 5b: Completely Clear Optical Fiber

Optical fibers can be polished with an optical fiber polisher like the one pictured in figure 6 below. This machine finely sands the corrupted parts of the optical fiber into two parts. The yellow sandpaper is more coarse and depletes the corrupted parts, while the green paper is finer and smooths the fiber after sanding the corruption off. The time it takes for fiber to become polished depends on the amount of corruption present. For reference, if a fiber is completely charred, polishing will take approximately thirty minutes to complete. Isopropyl Alcohol (IPA) is used as a lubricant and cleaner on the polishing machine and on the fiber tip itself.

An optical fiber is polished by first placing the fiber into the optical fiber guide. Then, a small amount of IPA is placed on the yellow sandpaper, and the machine is turned on. After the charred parts of the fiber are stripped off, the optical fiber and guide are placed on the green sandpaper to be polished. Finally, an IPA-soaked tissue is used to gently clean the fiber by twisting the fiber in a clockwise motion on the tissue. After polishing, an optical fiber microscope can be used to inspect the condition of the fiber.
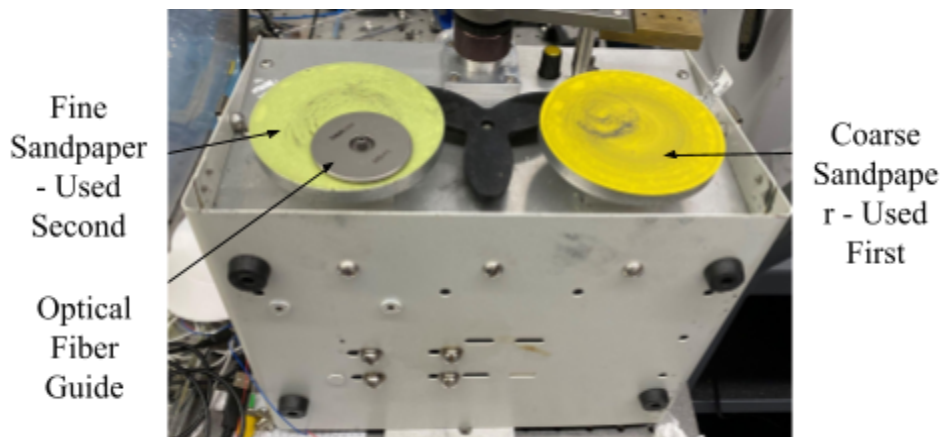
Figure 6: Optical Fiber Polisher

1.3 Existing optical coupling system in the lab for light coupling between fibers

In this section, we will explain the existing system in Professor Liu's lab that can couple light between two different fibers. We will explain the system components and their roles, as well as the working principles. The knowledge of this system serves as the starting point of our project.

(a)   (b)
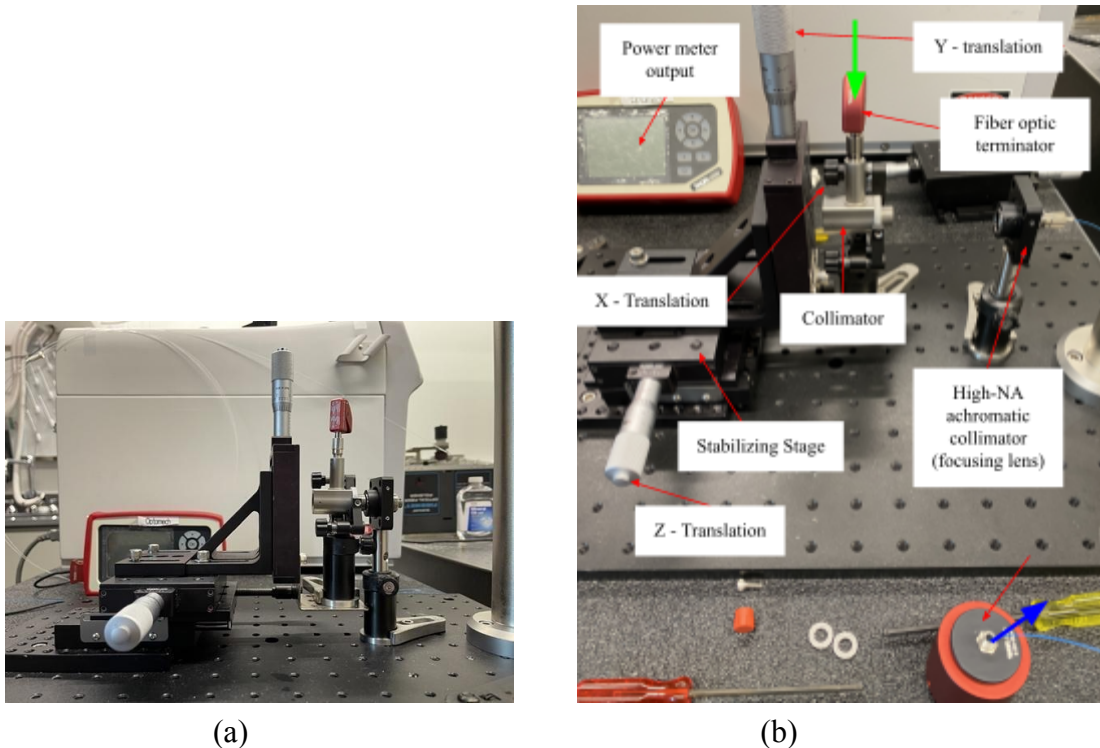
Figure 7 (a): Initial System Setup (b): Setup with labels

The initial setup of the system can be seen in figure 7 above. The large white box in the back of figure 7a is the medical laser. The metal components make up the stage as well as the alignment mechanism for the system. The red clip is where the medical endostat fiber is inserted into the coupling system. That clip is attached to a silver collimator that is able to collimate the light from the endostat fiber into a tighter column. That light is then sent to the black collimator to the right (figure 7b) which is able to refocus the light into a smaller fiber that can be inserted into a patient.

Collimators are a major component of our design. Understanding how they function can inform efficiency factors like alignment time because the angle at which light is collimated through each collimator is determined in part by how each collimator functions. With this information, the position and alignment of the collimation system are better informed, thus decreasing the necessary alignment time of our system.

A collimator is a device that narrows a stream of light into parallel rays [18, 19]. This is beneficial to focus the direction and efficiency of the light from the medical laser. Because the goal of the system is to channel light from one optical fiber to another, of differing sizes and modes, collimation is necessary to organize and direct the light. To create our free-space

coupling system, two different collimators are required. A depiction of this setup can be referenced in figure 7 below.
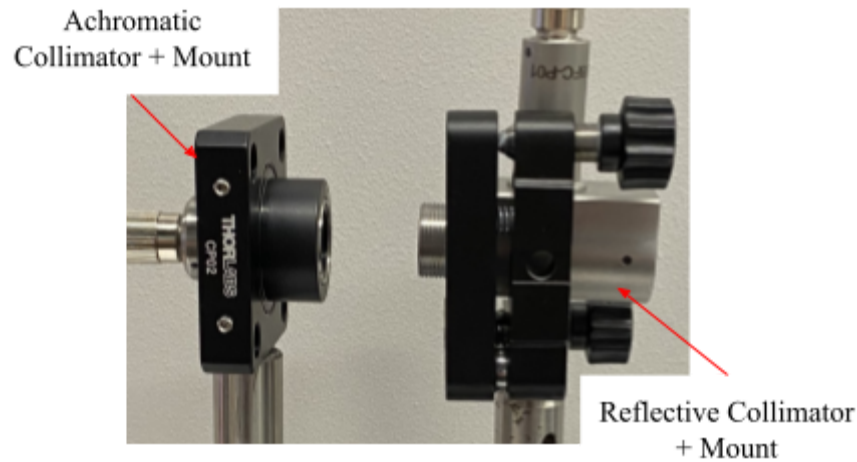
Figure 8: Close up of the collimators used in conjunction to create the coupling system.

The first collimator used is a standard, commercially available reflective collimator (figure 7a below). It acts as the conduit between the larger medical fiber input, and the free-space coupling system (see figure 1 above). This collimator utilizes an off-axis parabolic mirror to reflect the rays of light from the laser horizontally, no matter their position prior to reflection [20]. The reflective collimator used in the system can be seen in figure 9a below, and the inner workings of this system can be visualized in figure 9b below.

Figure 9a: Reflective collimator in system [20]   *Figure 9b: Reflective Collimator mechanism [20]*
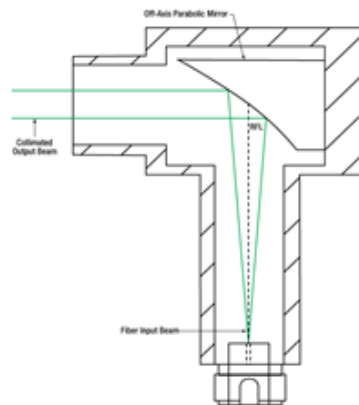
The second type of collimator used is a commercially available high-NA achromatic collimator for multimode fibers (see figure 8a). In our system, this collimator is held in place with a kinematic collimator mount adapter. This can be viewed in figure 9 below. This collimator launches the collimated light into the desired medical multimode fiber. This system consists of a meniscus lens to collimate the light and reduce spot size, and an achromatic doublet to bring

multiple wavelengths to the same focus [20]. The mechanism of this collimator is depicted in figure 9b below.

Figure 10a: High-NA achromatic collimator for multimode fibers used in system
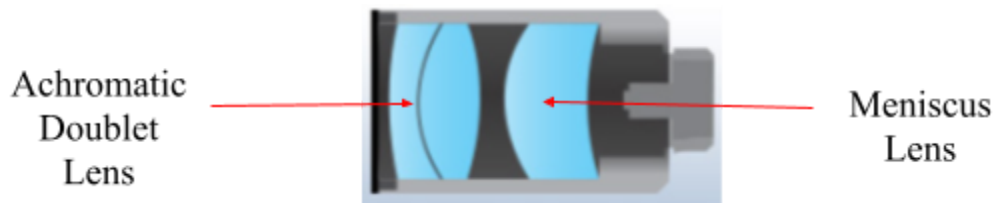
Figure 10b: Achromatic and meniscus lens mechanism for collimating to multimode fibers [20]

This free-space coupling system, created with the two collimators described above, is the mechanism for transferring the commercially available medical laser into a smaller, more flexible medical-grade fiber which seamlessly works within the mechanical endoscope portion of this design. By transferring the laser into the smaller fiber, the applications for this laser become boundless.

1.4 Medical Lasers

The final piece of this system is the medical laser. This project utilizes a 2004 Laserscope KTP/532 surgical laser. KTP lasers are solid-state lasers that use a potassium-titanyl phosphate crystal that directs an Nd: YAG laser to produce an intense green light beam at 532 nm [21]. This type of laser is used specifically for laryngeal surgery because the intense green light produced coagulates blood vessels which helps reduce the recovery time and increases the ease of the surgery [21]. Our specific laser model can also produce a red light which is used to determine the alignment of our system.

In addition to laryngeal treatment, this coupling system can be applied to various other procedures, leading to faster recovery rates for the patients and easier procedure protocols for the clinician.

1.5 Overall Goals and Contributions

This project builds on the work done by the WPI Optomechanics lab directed by Professor Liu in 2020, which is summarized in this paragraph. The team developed an optical fiber coupling system that couples a high-power (up to 20 W) surgical laser at 532 nm from a commercial medical laser source delivered by a 400 μm core fiber to a flexible and thinner multimode fiber for laryngeal surgeries with nearly 50 percent coupling efficiency [7]. In addition, the team validated the feasibility of removing tissue-mimicking agar at various optical powers (more extensive information regarding this process can be found in Chapter 4.4).

In this MQP, based on the existing system developed in these efforts, we extend the work in multiple frontiers, including the compactness and robustness of the coupling system, the improvement of the optical transmission efficiency, and understanding of laser-tissue interactions, all of which aim to enhance the system performance, user friendliness especially to non-engineers, and the feasibility of being used and maintained by healthcare professionals. Specifically, our efforts include creating an integrated and portable optical coupling system, efforts in feedback control of the optical alignment, parametric study of laser induced tissue damages, and study of laser induced cell damages. To report such a large project with diverse components, we would like to articulate our goals in this section before discussing any of the details in our work. We hope the readers can keep these goals in mind when going through the technical details, and we believe doing so will allow readers to grasp the importance of our work in an integrated manner, rather than be confused by the scattered details.

The overall goal of this project was to design an effective laser coupling system that can be implemented in clinical use to help physicians and patients. Our first goal was to improve the laser light coupling efficiency by improving alignment methods and collimator/fiber compatibility. Our second goal was to decrease the weight and size of the system setup to allow for easier incorporation into clinical use. A smaller, lighter, and more durable system will enhance clinical use. Finally, our third goal was to test the laser coupling system on biological materials and assess the damage. The completion of these goals characterize laser damage on tissue and contribute to the medical community providing evidence that more efficient laser systems can exist in the near future.

The ensuing chapters of this report are organized as follows: Chapter 2 discusses the design and realizations of the optical system. Chapter 3 considers the possible applications of the optical coupling system. Chapter 4 examines the characterization and results of the optical performance, biological tissue damage, and cellular tissue damage. Chapter 5 discusses these findings and highlights the growth and success throughout the project. Chapter 6 considers our future suggestions and regarding future work necessary to continue developing and improving laser coupling systems for surgical applications. Finally, Chapter 7 delves into the ethical and professional implications of our project.

Chapter 2: Design and Realization

Due to the current constraints of office-based laser surgery described in chapter 1, our team worked through numerous design iterations to create a smaller, portable, more efficient optical fiber free-space coupling system. Our goal was to incorporate these features into a system that will enable practical clinical use.

2.1 Goal and Specifications

Since the working environment of the free-space coupling system is the clinical office, the system should be portable to carry from offices to the operation room. The system should also be robust and easy to maintain. Based on the goal above, the initial specification of the system is summarized in Table 1-1.

We confined the dimensions of the system setup to smaller than 20 inches in length, 12 inches in width, and 8 inches in height; the total weight should not exceed 22 pounds. Initially, the transmission efficiency of the coupling system was under 40%. We aim to increase the transmission efficiency to above 65%. Another aspect we wanted to improve was the time and ease of alignment. While working with the system and decreasing its size, we have found the alignment of the system is very delicate. Alignment plays a major role in the output efficiency of the laser so it is important to ensure that the system is secure after the alignment has been set. We created designs with limited degrees of freedom because this decreased alignment complexity and increased the security of the system. Throughout the design process, we anticipated that the degrees of freedom can be removed, an ideal position can be established. However, we realized that some degrees are needed in the final design.

Table 1-1 displays the specifications of the initial design. The specifications of the second design iteration are displayed in table 1-2. These specifications further constrained the dimensions of the system to increase clinical use.

Table 1-1: Initial Design Specifications

abbr	Specifications
S1	product length < 20 in
S1	product width < 12 in
S3	product height < 8 in
S4	product weight < 22 lbs
	power transmission efficiency > 65%
S5	Current is 40%
	alignment should be reduced by 20% to 10 min
S6	current is around 15 min
S7	Fiber tip damage cycle increase 20%
S8	The material should be suitable for the system

Table 1-2: Revised Design Specifications

abbr	Specifications
S1	product length < 10 in
S1	product width < 9 in
S3	product height < 6 in
S4	product weight < 10 lbs
S5	power transmission efficiency > 65%
	Current is 40%
S6	alignment should be reduced by 20% to 10 min
	current is around 15 min
S7	Fiber tip damage cycle increase 20%
S8	The material should be suitable for the system

2.1.1 Design Loop

To fully develop a prototype that satisfies the objectives of this project, an iterative design process was used to modify and improve the current setup. The iterative methodology is summarized in figure 11.
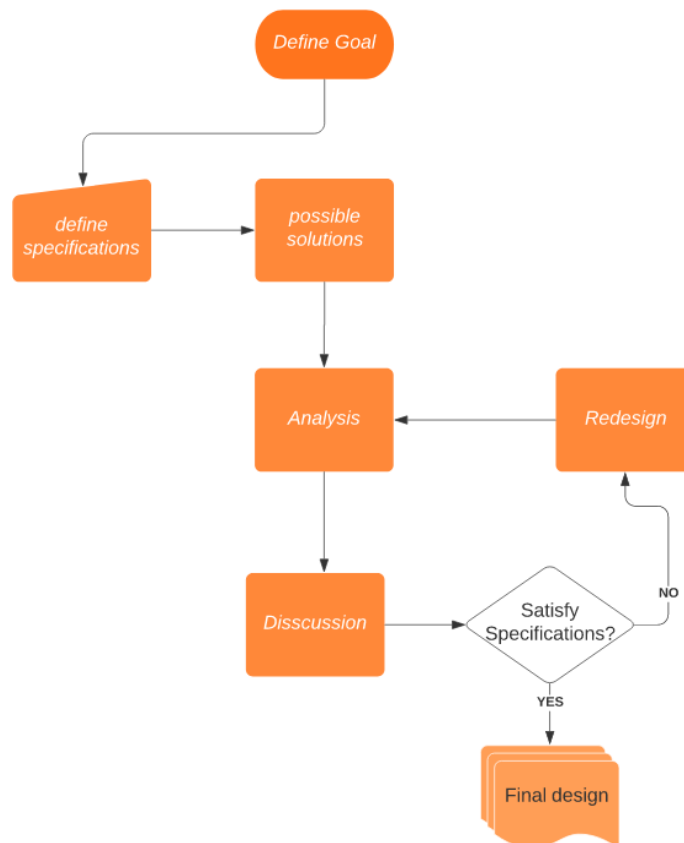
Figure 11: Iterative Design Process

Ultimately the goal of this iterative design process was to create an integrated and portable optical coupling system ready for clinic use. We defined a list of requirements and specifications of the system, then designed and developed possible solutions. Analysis and measurements were performed after each iteration to determine the feasibility of the design.

2.1.2 First Design Iteration and Assembly

The initial free-space coupling system (figure 12) was 16 inches in length, 10 inches in width, and 12 inches in height. The measured alignment time was about 15 minutes per period. Translation stages with micrometers in the X, Y, and Z-axis were included to ensure the collimator is horizontal to the mirror connected to the multimode fiber.

In the initial system setup, due to the height differences between two collimators, we assembled three translational stages, two metal boards, two metal hinges, and two posts in order to align the two collimators as well as to stabilize the system.
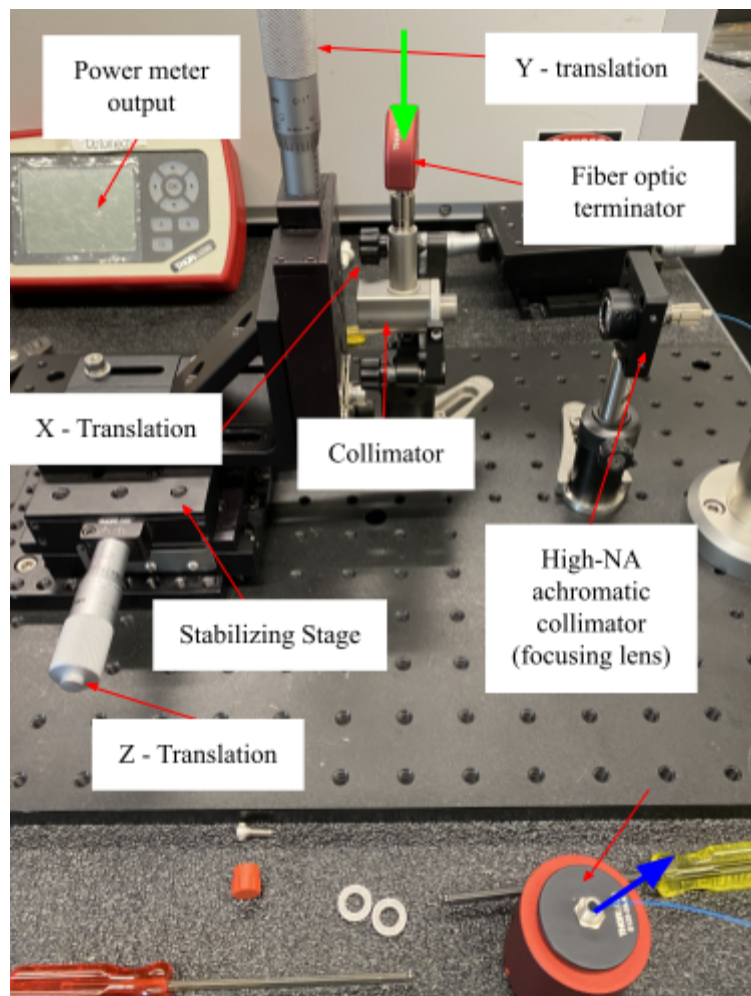
Figure 12: Initial free space-coupling system diagram. Here, the green arrow represents the medical fiber input, and the blue arrow represents the patient output.

Assembly:

Table 2-1 of the appendix includes all components and functions of the initial system. An image of the initial system can be seen in figure 13 below. We determined that although the dimensions of the initial system were relatively large for alignment and clinical use, the core part of the coupling system is only 9 inches.
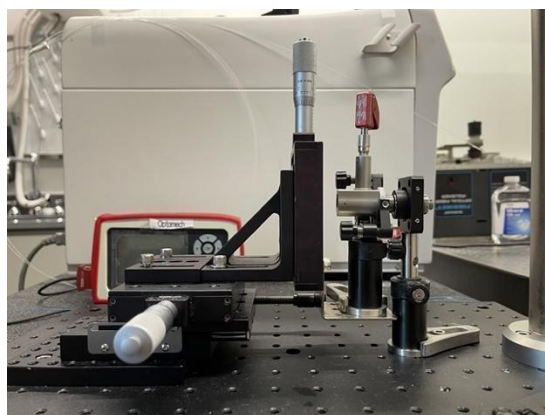
Figure 13: Initial System Setup

Table 2-1: Design Iteration 1 Results

Design #	weight(lb.)	efficiency	Alignment time	material
1	33	44%	10-30 min	aluminum

Summary:

In design iteration 1, we measured the estimated weight of 33 pounds with material aluminum, with maximum efficiency of 44% and an alignment time around 10 minutes to 30 minutes. We tested the efficiency of this system using the same efficiency testing procedure employed in previous design iterations. This method includes the use of placing the fiber optic tip into a power meter which outputs the power of the light in watts. As the results showed the weight and the alignment time of the first iteration design, there are some parts that can be improved to make the system better for clinic use. The key components are to reduce the size and to increase the power transmission efficiency of the system.

2.1.3. Second Design Iteration and Realization

Design:

The second iteration used smaller translation stages to make the coupling system less bulky. With this iteration, we decreased the size of the breadboard to 6 x 6 inches. Two long posts were used to align the collimator with the focusing lens. Although this design significantly decreased the size of the coupling system, it did not improve efficiency according to experimental results which can be found in table 2-2. Over time, the poles became slanted due to the weight of the

collimators which decreased the efficiency of the design. To preserve the alignment of the collimator and focusing lens, we designed a tube to aid alignment (see figure 14) and a casing for the entire coupling system (see figure 15).

Realization:

In this design iteration, we also eliminated translation in the y-direction, using a two-directional translational stage to leave the only translation in the x and z dimensions. In addition, the pole supporting the focusing lens was used to align the collimator and focusing lens in the y translation.

Figure 14: Second design iteration
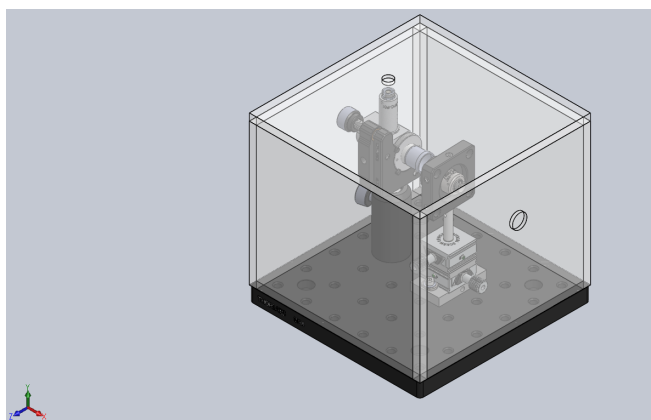
Figure 15: Second iteration design with casing
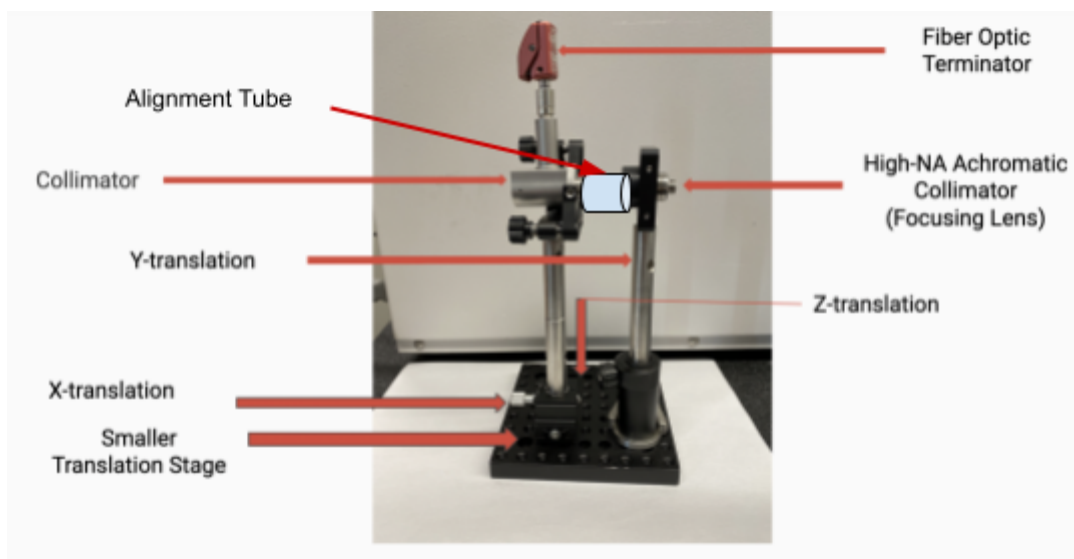
Figure 16:Realization of the second iteration
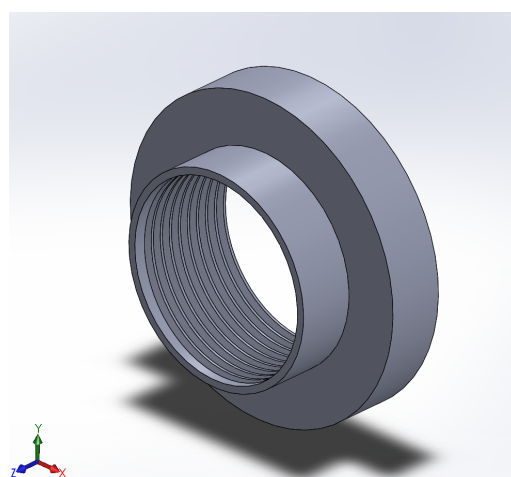
Figure 17: Alignment Tube design for second iteration

Table 2-2: Design Iteration 2 Results:

Design #	weight(lb.)	efficiency	Alignment time	material
1	33	44%	10-30 min	aluminum
2	17	25.14%	10-15 min	aluminum

Table 2-3: Design Iteration 2 Power Transmission Efficiency Results:

Set Up - Test #	Baseline Medical - Red	Patient output - Red (mW)	Baseline Medical - Green	Patient output - green (W)

	(mW)			(W)	
Setup #1-new					
1	1.75	0.25	0.70	0.176	
2	1.75	0.06	0.70	N/A	
3	1.75	0.08	0.70	N/A	
Setup #2 - previous					
1	1.75	0.48	0.70	0.48	
2	1.75	0.49	0.70	N/A	
3	1.75	0.42	0.70	N/A	

The small translation stages were used in design iteration two. This setup had an efficiency of 25.14%, while the initial setup had an efficiency of 48.57%. Therefore, the efficiency dramatically decreased with the smaller translation stage.

Summary:
Although the size of the system decreased drastically by nearly 90%, the power transmission efficiency also decreased by 23%. That amount of power lost is not ideal for the system and may cause a longer use period to get the same amount of output energy, which also indicates a shorter fiber tip damage cycle. After this design iteration, we were aiming to increase the power transmission efficiency since it's the non-negligible part of the entire system.

2.1.4 Third Design Iteration

Design:
After the second design was created, the deflection issue due to the height of the pole was discussed above. To correct this, we created the third design iteration. The patient fiber optic cable was changed for a smaller fiber in this design iteration. The previous fiber optic cable was 200μm in diameter, whereas the new cable was 125μm in diameter of the silica core. The new smaller cable consists of a glass multimode core that is wrapped in a thick plastic jacket. We hypothesized that a smaller cable would be able to fit and bend inside an endoscopic metal casing better than the thicker fiber. This is because there is less material to push back on the metal casing, meaning the fiber will be able to achieve a greater bending angle.

Table 2-4: Design Iteration 3 Results

Trial	Baseline	Patient	Patient	Baseline	Patient	Patient

Number	Medical - Red(mW)	Output - Red (without tube)(mW)	Output - Red (with tube)(mW)	Medical - Green(W)	Output - Green (without tube)(W)	Output - Green (with tube)(W)
1	1.84	0.355	0.323	0.67	0.13	0.12
2	1.86	0.665	0.265	0.70	0.26	0.10
3	1.82	0.49	0.333	0.71	0.19	0.13
Avg	1.84	0.50	0.307	0.69	0.19	0.12

Table 2-5: Design Iteration 3 Results with New Fiber

Trial Number	Baseline Medical - Red(mW)	Patient Output - Red (Old Fiber)(mW)	Patient Output - Red (New Fiber)(mW)	Baseline Medical - Green(W)	Patient Output - Green (Old Fiber)(W)	Patient Output - Green (New Fiber)(W)
1	1.84	0.355	0.35	0.67	0.13	0.13
2	1.86	0.665	0.45	0.70	0.26	0.10
3	1.82	0.490	0.65	0.71	0.19	0.13
Avg	1.84	0.50	0.48	0.69	0.19	0.12

Summary:
In the third iteration experiment, we tested the function of the tube between two collimators and a 125 μm diameter fiber. There was no clear increase in the transmission efficiency with the existence of the tube compared to the data gained without the tube. All results from the efficiency tests via power meter can be seen in Table 2-4 above.
We also tested the new fiber with a 125 μm diameter to ensure its feasibility. The results showed there was no clear increase in the efficiency for the laser at both of the given wavelengths. The data is presented in Table 2-5 above.
Since there was no clear sign of the feasibility of the tube and the 125μm optical fiber, we decided to no longer consider these two parts in future iterations.

2.1.5 Fourth Design Iteration and Realization

Design:
The fourth iteration focused on fixing the lack of stability, size, and alignment present in the previous design iterations. Because the 3D printed tube (as seen in the second design iteration above) added no efficiency to the system, we did not include it in the fourth design. The hallmarks of this design include directly connecting the high-NA achromatic collimator to a small-scale translation stage. We also chose to omit z-translation for the reflective collimator by removing the sliding post used in previous designs.

We determined that this design would be more effective than previous attempts because it cuts down on the overall size and lack of stability of the system. Positioning the collimators closer to the base of the design also increased the stability of alignment and positioning of the lenses inside the collimators. This was a necessary improvement because as determined in previous iterations, very fine movements of the lenses can result in noticeable differences in the efficiency of the system. We hypothesized that this more compact position would allow for a more secure placement of each collimator so that maximum efficiency can be realized.

Realization:
To test this new design iteration, we utilized on-hand equipment and parts from previous designs including two 2-directional translational stages to create a rough prototype of the fourth design iteration. A diagram of this setup can be seen in figure 16 below.
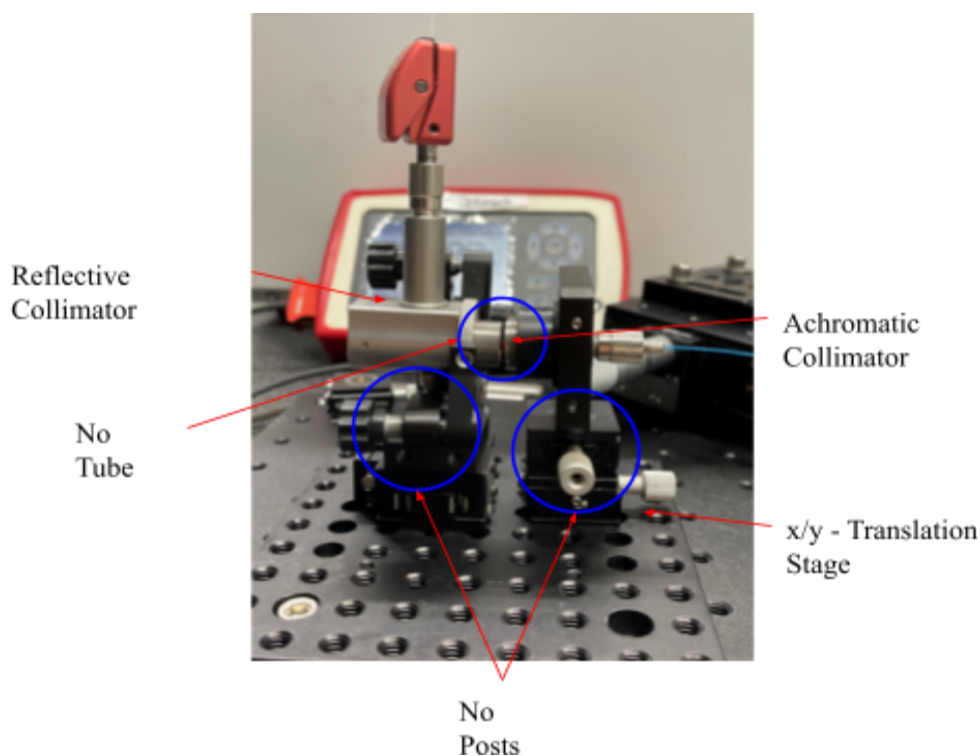
Figure 18: Fourth design iteration

Summary:
Through this testing, we determined that the fourth design iteration did not greatly affect the efficiency as the values for power output were similar to those found in previous designs. However, the size, ease of alignment, and stability of positioning were noticeably improved. The results of these tests can be found in Chapter 5.

2.1.6 Fifth Design Iteration and Realization

Design:
Because the prototype testing for the fourth design iteration did not result in great efficiency improvements, the team decided to create an alternative to this design iteration using Solidworks (see figure 17 below). This design includes an extra z-translation stage that connects to the x/y-translation stage on the achromatic collimator. The team hypothesized that an additional translation stage would increase the alignment capabilities of the system, which would theoretically increase efficiency.
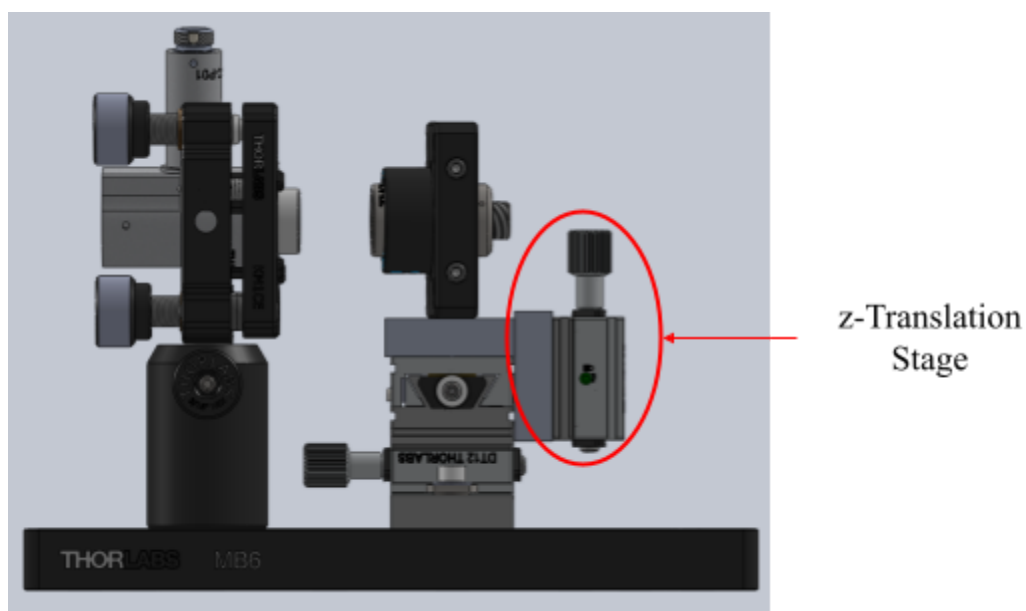
Figure 19: Alternative to the fourth design iteration

Table 2-6:Design Iteration 5 Results

Trial Number	Baseline Medical - Red(mW)	Patient Output - Red(mW)	Baseline Medical - Green(W)	Patient Output - Green(W)

| 1 | 1.98 | 0.323 | 0.67 | 0.12 |
| 2 | 1.98 | 0.389 | 0.67 | 0.26 |

In design iteration 4 testing, we aimed to prove the increase of efficiency without the existence of the long posts. But at this point, we determined that the power meter we used to measure this data had drifting issues that were caused by an electronic short circuit. Therefore, we cannot ensure the validity of this data and must assume it is inaccurate.

Summary:
Ultimately, the team decided against fabricating this design. Through analyzing the efficiency data gained from the prototype, and by weighing the pros and cons of the design improvements made in Solidworks, we determined that along with limited time and monetary funds, the advantages of this new design could not improve the efficiency enough to justify fabricating this design.

2.1.7 Sixth Design Iteration and Realization

Design:
Based on the obstacles we had in the previous design iterations, along with the fact that the two collimators have different heights; it was difficult to keep two collimators levels. As a result, we came up with a custom L-stage design that has different heights at two ends of the plate. One side is higher than the other to make sure the two collimators can align with each other without extra posts to support them. They can be directly connected to the stage with the same size hole at the bottom. This design can be seen in figure 18 below.

We also measured the most efficient power transmission position (see figure 18) to determine the positions of two collimators since this iteration does not include any translation stages.

Realization:
Without the original breadboard, posts, and post holders, the weight of the entire system has been decreased drastically. We chose an aluminum material for the L-shaped stage, with an estimated weight of 0.25 pounds to make this design as light as possible.
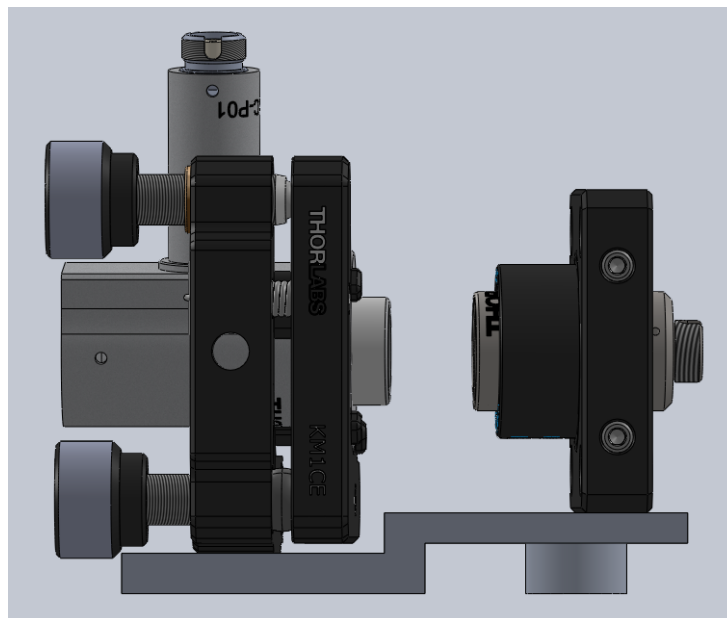
Figure 20: Final Iteration for E2

Design Iteration 6 Results:
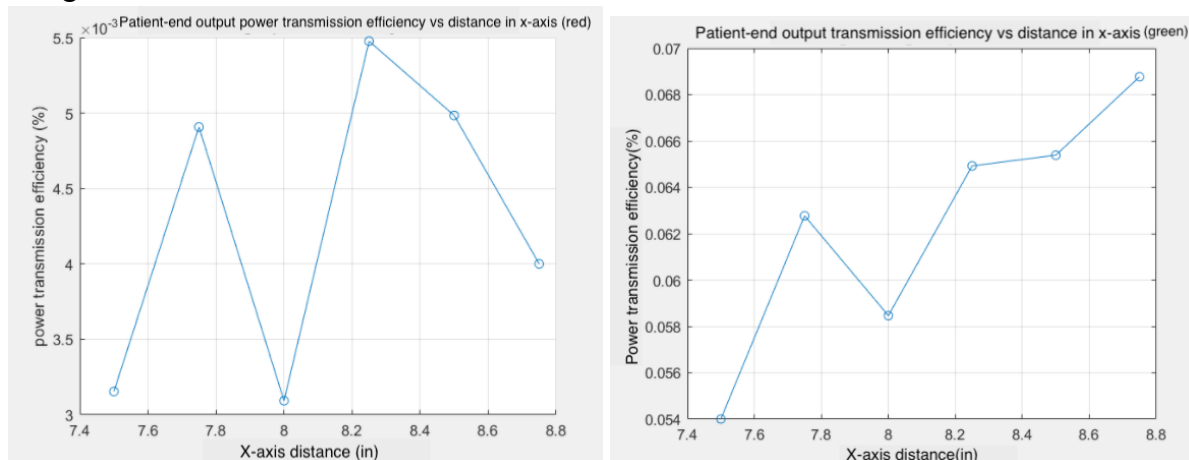
Figure 21: Design Iteration 5 Results

Summary:

In design iteration 6, we measured output power transmission efficiency at multiple positions on the x-axis from the beginning of the optical breadboard to find out the position with the maximum transmission efficiency. The x-axis of the plot is the x-axis positions measured from the beginning of the coupling system with the other collimator fixed. When the two collimators are closer to each other, the power transmission efficiency of the green light is higher than during other conditions.

2.1.8 Testing prototype on design iteration 6: X-Y, X-X, Y-Y Directional L-stage

At the beginning of the A term, we were focused on fabricating and testing the L-shape stage based on the final design iteration in E2. Rather than fix the x and y positions, we determined that alignment along the x and y-axis on the L-stage would be beneficial to transmission efficiency.
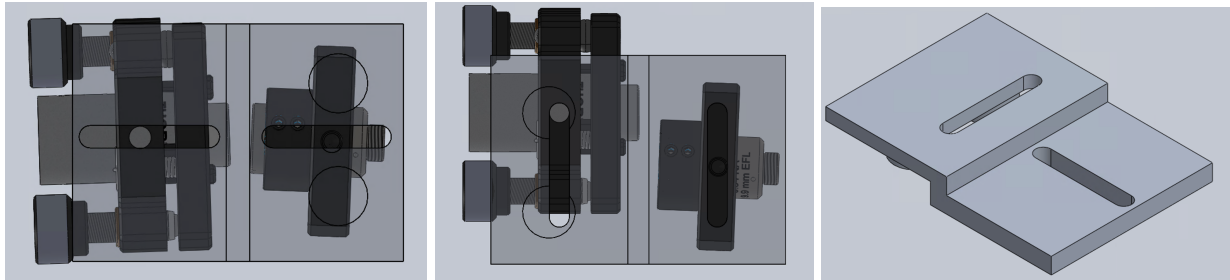
Figure 22(a): Y-Y directional L-stage   *Figure 22(b) X-X directional L-stage*   *Figure 22(c): X-Y directional L-stage*

In order to get more comprehensive measurements, we decided to utilize stages with different translation axis slots. We cut two slots in the x and y-axis respectively on both sides of the stage. In addition to the x-x and y-y stages, we also implemented the x-y stage which takes one translation slot in the x-direction, the other one in the y-direction.

Fabrication:
We fabricated the L-stage with the 3D Printing machine and specific material to ensure the strength to hold each component to prevent them from shaking.
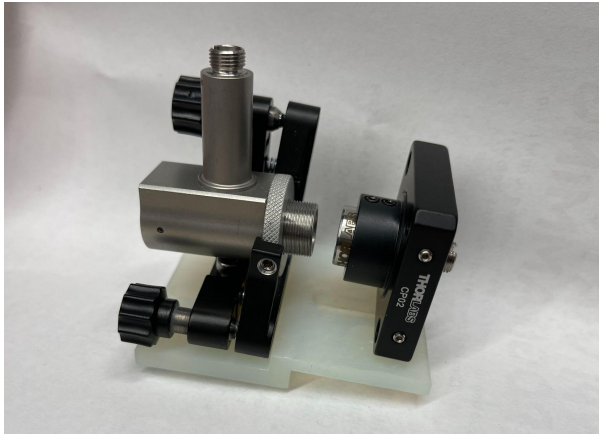
Figure 23: X-X directional L-stage prototype   *Figure 24: X-Y directional L-stage prototype*
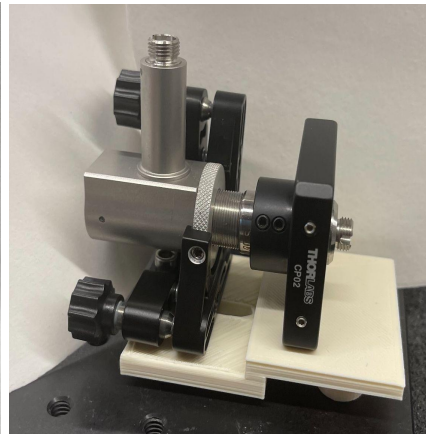
When we were assembling and testing the L-stage prototypes, we noticed some design limitations including the screw-nut at the bottom of the stage, which made the stage unstable, and the center of the two collimators was not aligned, which means the x-position of the slots was not precise. In the next iteration (Figure 24) we modified the prototype to include a revised

height of the support cylinder under the right side (higher) stage and recalculated more precise slot positions.

Summary:
The results we got from the X-X and Y-Y directional stage design were not ideal and only provided 20% transmission efficiency on green light due to the limitations we mentioned in the design iteration section.

For the X-Y directional stage design, after we addressed the limitations the efficiency increased by 20.9% for the red light. We tried to align the system with the green light to gain the most precise alignment and it caused burning on both end faces of fiber tips which affected green light transmission efficiency results.

The detailed testing results of L-stages designs can be found in Chapter 4, table 4-1and table 4-2.

2.1.9 Design iteration 10: Z-directional L-stage Testing prototype
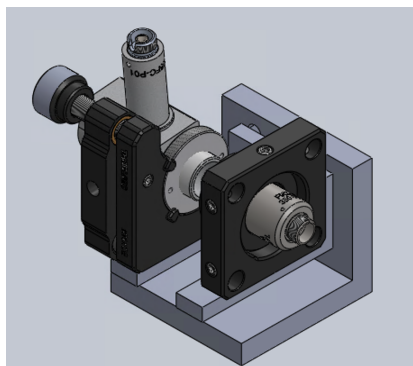
Figure 25: Z directional L-stage CAD   *Figure 26: Z directional L-stage prototype*   *Figure 27: X-Y directional L-stage prototype with translational stage*
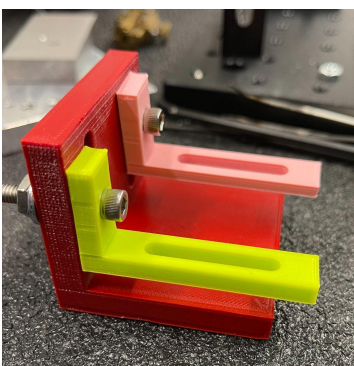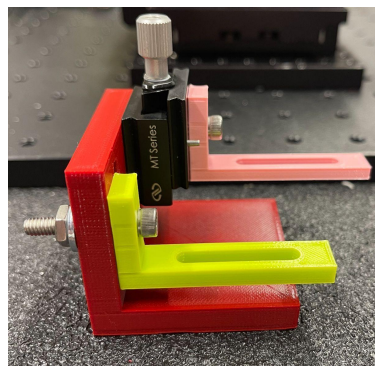
Besides the x and y directional testing stage, we also developed several z directional testing prototypes to analyze z-direction alignment and collect data that could be used to determine the fixed metal L stage design.

Fabrication:
We created each part of the system by 3D printing for testing purposes. At first, we designed a larger L-shaped plate on the x and z plate (red plate in Fig 26), two smaller stages (green and pink stages) to hold two collimators. We found imperfections of the design that made the prototype less efficient such as wobbling stages due to the length of the slots in the larger plate and the smaller stage on the left side not being able to hold the collimator stable.

Summary:
Due to the limitations mentioned before, no data was collected with this prototype. But in order to improve the limitations, we attached a miniature translational stage with one of the smaller stages, which led to the next iteration.

2.1.10 Design iteration 11: Z-directional L-stage Testing prototype iteration II

Design:
In addition to one translational stage in the z-direction, we explored multiple direction alignments in the same design. We revised the previous design iteration, incorporating an extra translational stage in the x-direction to obtain more accurate results. To better secure the collimators to the smaller stage, the width of the L-stage was decreased.

Based on the results from z-direction and x-direction testing, which will be discussed in the next chapter, we fabricated the first metal L-stage with fixed positions on top. The fixed positions on the metal stage did not result in great efficiency, therefore, we determined that the metal plate fixed position design iteration was not sufficient.

Fabrication results:

We 3D printed the three L-shaped stages with higher density material to ensure the robustness of the testing prototype (see figure 28 and 29). Figure 30 depicts the metal L-stage fabrication. We cut the L-stage metal piece and drilled the holes for screws with a CNC machine to ensure the precise location and make sure two collimators will align perfectly.
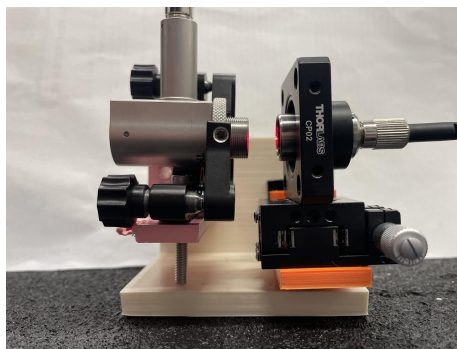
Figure 28: Z directional L-stage prototype II front view
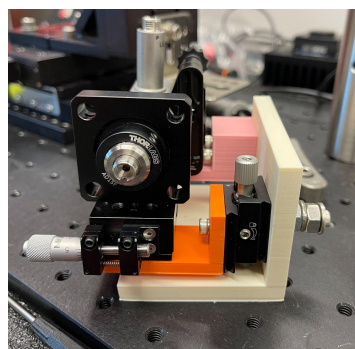
Figure 29: Z directional L-stage prototype II top view

Figure 30: Metal L-stage fabrication

Summary:
The testing results from the Z-direction design iteration II increased from 18% to 37.8% compared to the fixed stage setup. This data reflects the importance of the stability of the system. We focused on testing the red light efficiency because we were able to run consistent red light tests without compromising the efficiency of either fiber. Through this we achieved a maximum of 37.8% transmission efficiency. More data is presented in Table 4.1.4.

2.1.11 Design iteration 12: X-Y-Z-directional L-stage Testing Prototype

Design:
Based on the testing from the fixed positions on the metal stage which did not result in great efficiency, we changed the fixed position idea on the metal plate and kept testing alignment on all X-Y-Z directions. We revised our design to incorporate a single axis translational stage

attached in the z-direction, and an X-Y multi-direction translational stage with the collimator on the left side. At first, we wanted to keep all translational stages on one collimator then we noticed it was difficult to align two collimators properly due to the weight with respect to the translational stages.
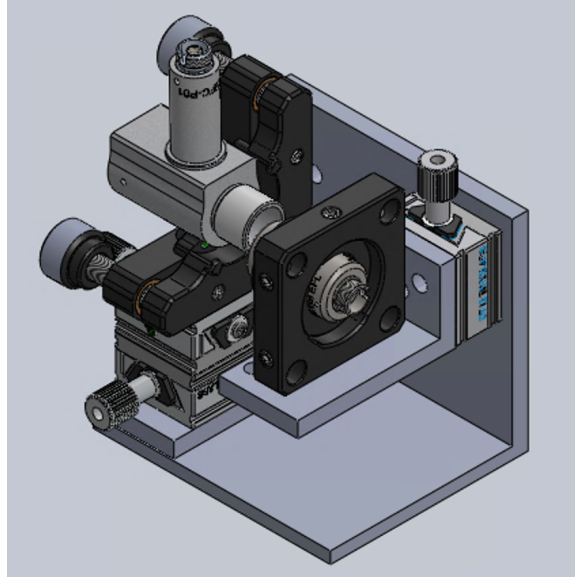
Figure 31: X-Y-Z-directional L-stage testing design iteration I

Assembly:

Based on the idea from the previous iteration, we assembled the next iteration with available components in the lab. Attached is the X-Y multi-direction translational stage on the breadboard at the bottom and used the L bracket to hold the translation stage in the z-direction and connected with the collimator. This iteration with metal boards was more stable than 3D printed stages, all translational stages worked well enough to see an increase in the efficiency results.
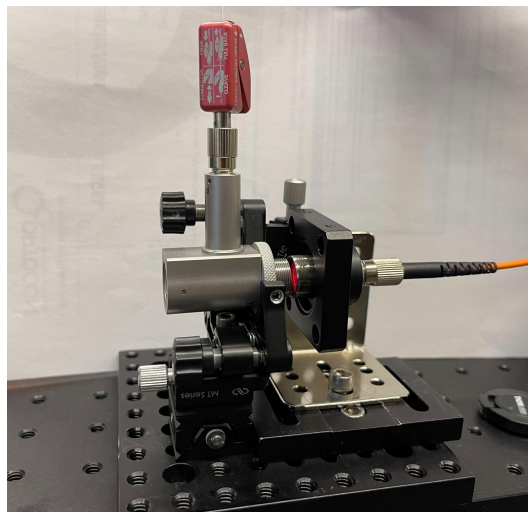
Figure 32: X-Y-Z-directional L-stage testing design iteration II

Summary:
The testing result from X-Y-Z directional L-stage testing design iteration II shows the best result we got through the term. We got a maximum of 50% transmission efficiency for red light and a maximum of 53% for green light. Due to the stability feature for metal boards in the prototype, we were able to perform fine alignment in all x,y, and z directions. We aim to get better transmission efficiency when we test the new collimator on this setup. (Table 4-5)

2.2 Optical Components

2.2.1 Optical Components optimization and investigation

Optical components are one of the most important parts of the system. As mentioned in chapter 1, the collimators will determine how much the power of the laser beam will couple to the medical patient fibers. There are two collimators in the system. One is connected with the medical endostatin fiber, which will be considered as an input collimator. The other one is connected with the output medical patient fiber, which is called output collimator.

Improving the total power transmission efficiency is one of the goals of this project. We tried to reconsider the choice of optical components in the system. There are several factors and parameters of the collimator we took into consideration including desired wavelength, output beam diameter, and numerical aperture(NA). At first, we thought we should match these two collimators with the parameters. But we could not find any available collimators from the manufacturer and found out that was not in the right direction either. Then we aim to match the collimator with its corresponding optical fiber. The differences between the collimator and fiber should be minimized in terms of NA and output beam diameter. With the help of the technician from Thorlabs, we chose two collimators with the better match in terms of the NA and output beam diameter.

Table 2-7: Input collimator Comparison

	New collimator	Original collimator
Part number	F240APC-532	F950FC-A
Design wavelength	532 nm	486 nm, 588nm, 656 nm
Output beam diameter	1.48 mm	4.5 mm
Numerical aperture	0.51	0.54
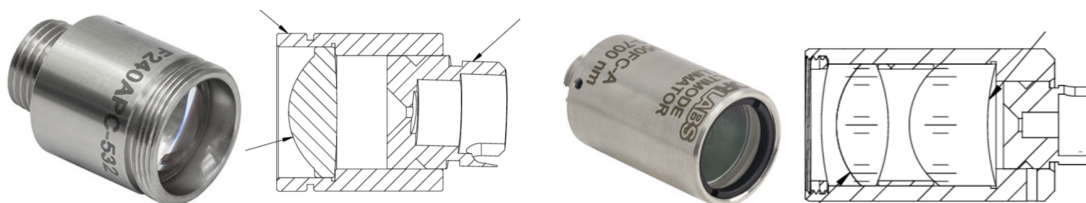
Figure 33: New input collimator (Left) and original input collimator (Right)

Table 2-8: Output collimator Comparison

	New collimator	Original collimator
Part number	RC02FC-P01	RC08APC-P01
Design wavelength	450 nm - 20 μm	450 nm - 20 μm
Output beam diameter	2 mm	8.5 mm
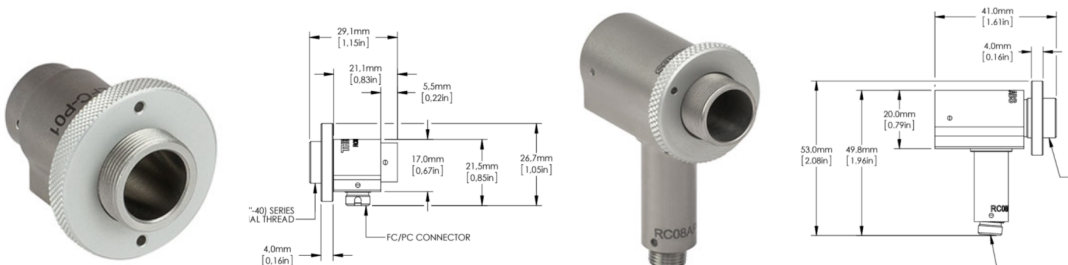
Figure 34: New output collimator (Left) and original output collimator (Right)

2.2.2 Auto-calibration stage

At the end of the design process, after a few months of testing the system setup, we found out the most inefficient part of the entire system was to get the alignment perfectly to achieve the most efficient position. The alignment time usually takes 15 to 20 minutes. It will make the alignment process much more efficient and easier if there's an auto-calibration system based on feedback control. This is especially meaningful, considering this system will be potentially used and maintained by healthcare workers, not engineers.

So we performed the feasibility study on the auto-calibration stage. The auto-calibration stage includes a motorized probe, a one-directional translational stage, and a thermal sensor power meter (Digital handheld optical power and energy meter console, item number PM100D, ThorLabs) to read the output of the medical patient fiber. We implemented a control loop to calibrate the motorized stage to obtain the most efficient power transmission position.
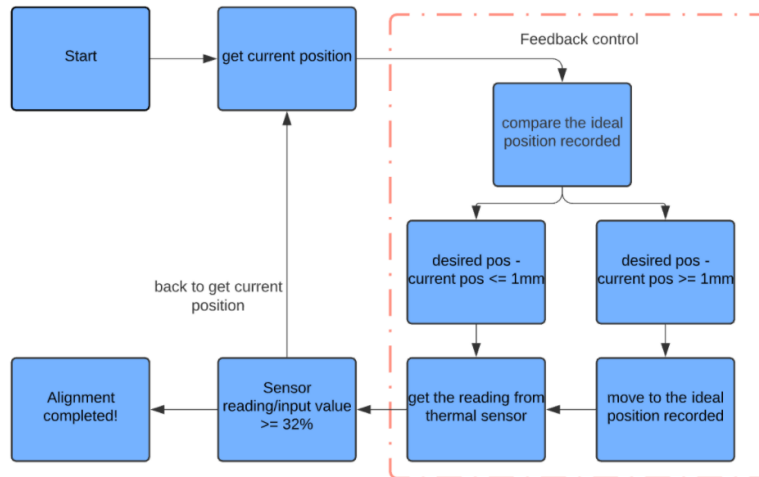
Figure 35: Feedback control loop diagram

The system will start to get the current position either using LabView or Matlab. Then in the feedback control loop, the system will compare the ideal position recorded by manual alignment. If the difference between the desired position and the current position is greater than 1mm, the stage will move to the ideal position recorded and then get the reading from the thermal sensor. If the difference between the desired position and current position is less than 1mm, the system will get the reading from the thermal sensor. If the sensor reading is greater than 32%, which is the greatest power transmission efficiency when we performed the testing before the final system, the alignment is completed and the system is ready to use. Otherwise, if the sensor reading is lower than 32%, the control loop will restart to get the current position.

Although due to the time limitation, we did not collect more data to show a fully functional automation system. But the general idea will help us to save time and energy from aligning the system with the best power transmission efficiency, and this work provides a good start point for future work.

Chapter 3: Literature Review of Laser Coupling System Applications

Because the free-space coupling system passes a common medical-grade laser through a small flexible optical fiber, there are many different medical applications for this system along with laryngeal surgery. To better understand the impact of the laser on biological tissues for further application, it is necessary to quantify the damage this laser system does to regular, healthy tissue. This effort is important in our MQP not only because the fundamental understanding and experimental data of laser-induced tissue damage are limited, but this work serves as an ideal way to demonstrate the clinical potential of this MQP developed laser coupling system. In this chapter, the team will summarize the information we got from the literature for the potential applications of our coupling system, and none of our own experimental work is included here. Such information allows us to determine proper ways to demonstrate the applications of our system, which will be detailed in Chapter 4.

Recent work on the simulation of a steerable fiber demonstrates nearly 70 percent more reachable area across larynges compared to straight fiber [6]. This comparison shows that the steerable fiber is able to treat patients whose lesion locations were complicated that cannot be treated before. One major constraint is the lack of suitable fibers. The ideal fiber requires minimized diameter and bending radii in order to reach certain areas of the larynx. However, commonly used medical lasers (PDL, CO2, KTP) have thicker fiber cores (>0.4mm diameter) [8] and caused larger bending radii (>3cm), which results in limited steering angles thus not appropriate to bend inside the narrow larynx [8]. In addition, the effect of the laser on biological samples should be further investigated to validate that the coupling system design can meet the user needs and the design requirements. The following sections will outline possible further applications of the laser coupling system as well as the background needed to understand it.

3.1 Testing Damage on Skin

While the testing of this specific free-space coupling system is not well documented in literature, procedures to quantify medical laser damage on healthy biological tissues have been thoroughly explored. Given that our laser system is intended to be used on human patients, we have an ethical responsibility to clinically prove the damage it may cause on biological samples.

By conducting a thorough literature review on quantifying tissue damage via medical lasers, three main methods came to light. These methods include completing a thermal damage calculation [22], assessing the damage via macroscopic and histologic observation via dyes, microscopes, and imaging software [23, 24]; and utilizing bioluminescent imaging to detect thermal stress [30]. Of these three methods, the most feasible and replicable method was determined to be the thermal damage calculation, along with some macroscopic and histologic observations. This method involves calculating the thermal damage via the Arrhenius equation. Because there are multiple independent thermodynamic processes associated with laser ablation, the Arrhenius equation is ideal to find the thermal reaction rate to assess thermal damage because it allows for multiple independent processes to be studied in parallel [27]. The Arrhenius Equation below (figure 34) can be derived to show that the laser power, the spot moving speed, and the pulse frequency determine the thermal damage parameter, Ω. These independent variables can be found using the process pictured in figure 8 below [22].

Figure 36: General method for thermal damage calculation [22]

In this equation, A is the frequency factor, E_a is the activation energy, T is the thermodynamic temperature, and R is the universal gas constant. The thermodynamic temperature can be found by using a simple temperature-time fitting curve.

$$\Omega = \int_0^t A e^{-\frac{E_a}{RT}} \, dt$$

Figure 37: The Arrhenius Equation

Because our lab already houses all the materials to conduct this procedure, it is the most feasible option for quantifying laser damage on biological tissues. The team decided to conduct tests on pig ears, pig larynxes, and cell samples. The pig ears and larynxes were acquired from Adams Slaughterhouse. With this testing, we observed and analyzed the energy put into the system vs. the damage done on the sample. The results and discussion from these experiments can be found in Chapters 4 and 5.

3.2 Photodynamic Therapy

Testing the damage of the coupling system on healthy tissue will determine how feasible it is to use on surface ailments like skin cancers, lesions, or cysts. By outputting less power throughout the system, or with the use of different wavelengths, photodynamic therapy can be a therapeutic

application for this system. Photodynamic therapy is a non-invasive form of treatment for non-oncological and cancerous diseases which utilizes a photosensitive compound and specific wavelength to denature cancerous or unhealthy cells [26]. Presently, the treatments available for cancerous diseases are toxic to not only cancer cells, but also healthy cells. Treatments like chemotherapy have numerous painful side effects, therefore, it is important for the betterment of society to create a more effective, less toxic treatment for cancerous diseases [26].

Photodynamic therapy is well researched and documented in the literature, and many mechanisms have been created to carry out this type of treatment. The most feasible method for our type of laser supported by literature is photodynamic therapy, supported by electroporation. Electroporation is a technique that reversibly unseals cell membranes so that a photosensitive compound (like chlorine e6 and AlPcS4 - phthalocyanine) can be introduced to the cell [26]. Once this occurs, healthy cells and cancerous cells will uptake and incubate the photosensitizer. The photosensitizer will accumulate in cancerous cells at a much higher concentration than in healthy cells. Therefore, when the waves from the red light laser penetrate the cancerous cells versus healthy cells, a photo cytotoxic reaction occurs in only the cancerous cells due to the biodistribution of the photosensitizer, aided by electroporation [26]. A depiction of this mechanism for photodynamic therapy can be seen in figure 37 below.
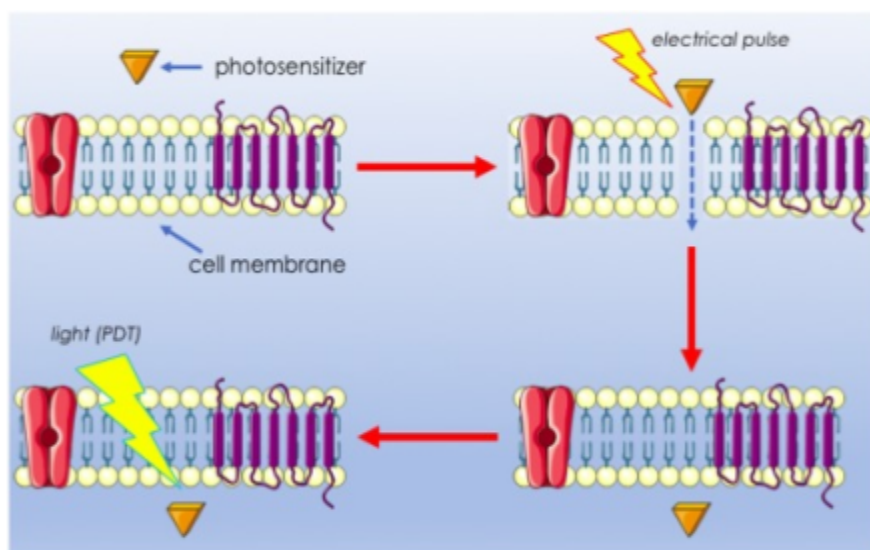
Figure 38: Photodynamic Therapy - Supported by Electroporation
[26]

While this process is quite technical, there are U.S. labs that supply the necessary materials to test if our Nd: YAG laser can carry out photodynamic therapy [31]. Once this is determined, the portable, flexible nature of our optical fiber system could make photodynamic treatments more accessible and broaden the applications of photodynamic therapy to previously inaccessible, or untreatable cancers.

3.3 Breast Cancer

This laser coupling system might also be able to treat small tumors. Invasive and in-situ tumors may be percutaneously ablated by a stereotactically guided laser needle and subsequently evaluated by imaging methods and needle biopsy [12]. A recent study stereotactically guided an 805 nm laser beam via fiber in a 16G needle delivered to cancer. The tumor size ranged from 5 mm to 23 mm with an average size of 12 mm. The experiment indicated that for 100% tumor coagulation, 1,400 joules of laser energy per cubic centimeter of the calculated tissue are needed. Furthermore, the study reported that in order to reach full death of the tumor cells a temperature of at least $60℃$ ($140℉$) has to be attained. Using percutaneous laser treatment to eliminate breast cancer is better for the patient as the treatment is targeted directly to the tumor and does not have to affect all the cells in the body the way chemotherapy and radiation do. Figure 12 below shows how a laser needle is inserted into the center of the tumor through a small skin nick and a multisensor thermal needle through a second nick. This is a less invasive alternative to open surgery for a subset of mammographically detected breast tumors. In order to pursue this type of testing, we can order cancer cell lines and combine this testing with photodynamic therapy. As a result of the thorough research that has been conducted and the literature that has been produced regarding this type of treatment for breast cancer and photodynamic therapy, our research and testing would be allocated better towards other directions where our coupling system can produce new results.
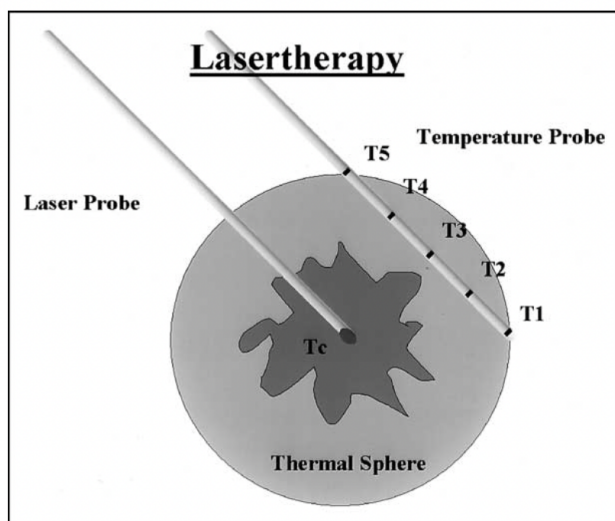
Figure 39: Laser and temperature probe in breast cancer [12]

3.5 Tonsillectomy

In addition to bone cutting, this laser could be used as an alternative to how tonsillectomies are usually done. Tonsillectomies are typically performed by cutting out the tissue and then cauterizing all the blood vessels in the area. Patients need to be put under and often experience severe pain and sometimes bleeding after surgery, requiring more surgery. Using a laser to kill the tissue while also cauterizing the area would make for a quicker procedure, as well as one that

only requires local anesthesia [15]. Overall, the surgery would cost less, and make for better recovery for the patient. There has been a considerable amount of research on this new method for tonsillectomies and it seems promising. The system we hope to create would give clinicians the advantage of being able to precisely navigate the small area in the mouth as well as decrease complications and surgery time [16].

3.6 Acupuncture

While not a surgical approach, coupling acupuncture needles with our free-space coupling system could significantly increase the effectiveness of acupuncture treatments. Acupuncture treatments coupled with low-level laser therapy have the potential to treat musculoskeletal conditions.

Ultra low Level laser therapy has been used to treat musculoskeletal conditions and associated motor functions. It is well documented that low-level radiation promotes cellular redox reactions. When a low-power (max of 7 mW) laser with a wavelength of 650 nm (red light) was locally applied to an area with musculoskeletal pain, cellular redox reactions occur in the extracellular soft tissue matrix (ECM). The flow of photons through the ECM creates similar metabolic conditions to normal, thus decreasing the nociceptive stimulus that causes musculoskeletal pain [33]. Coupling acupuncture needles with our laser device would primarily ease the implementation of low-level radiation by localizing the application of light. Furthermore, our coupling device already has the capacity to emit red light at low power, making the transition from other medical applications quite feasible.

The only drawback mentioned in the reviewed literature about laser therapy for acupuncture is that there is only a small window in which the laser light is effective to induce the biochemical reactions required, which can be seen in figure 40 below [33]. While this is an issue, it is possible to design a system that could overcome this challenge.
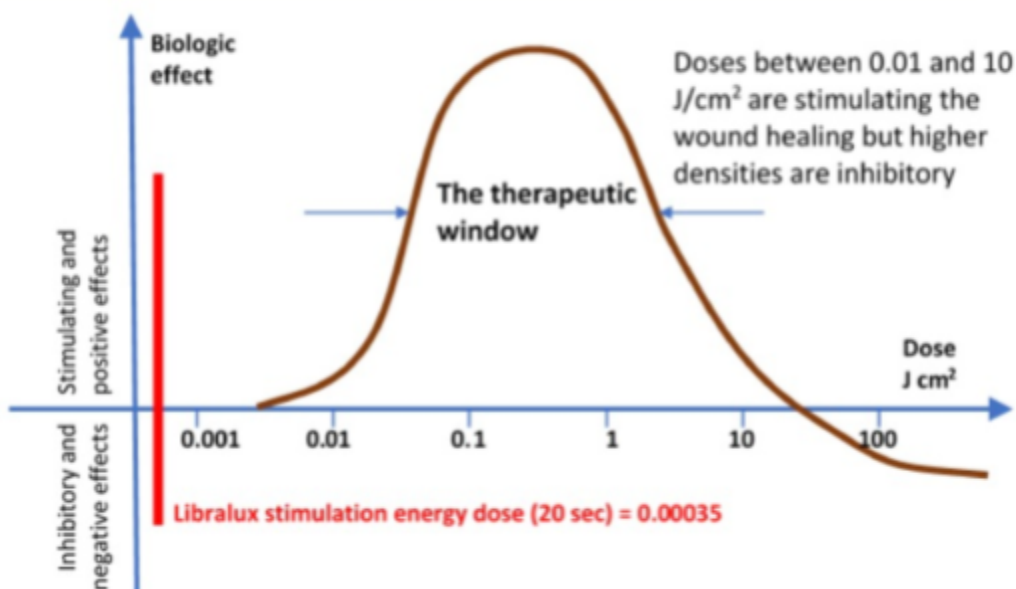
Figure 40: Graph that depicts the small window of therapeutic laser energy (in J cm^2) [33]

Another advantage of pursuing this application is that we have access to many of the necessary materials needed. One way to study the effects of our laser system on necessary biologic processes is to monitor the neurite elongation as well as the mitochondrial membrane potential. To carry out this process, one would need to purchase mammalian neural cell lines, the mediums necessary to culture these cells, and JC1 vital dye to monitor mitochondrial membrane potential [34]. One would also need to utilize some equipment that already exists in the lab including the laser-confocal microscope and the cell culture hood. An example of this experimental setup can be seen in figure 39 below [34].
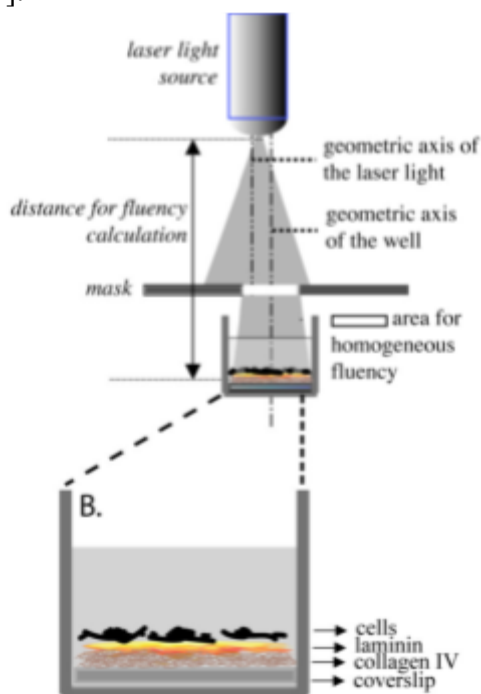
Figure 41: Laser setup for neurite elongation and mitochondrial membrane potential [34]

The main goal of carrying out this procedure would be to determine if our laser system is able to replicate the neurite elongation and mitochondrial membrane potential experienced during cellular redox reactions that decrease nociceptive stimulus. If so, one can determine that our system is capable of decreasing musculoskeletal pain, and can deliver more effective acupuncture that could greatly impact pain and motor dysfunction.

3.7 Summary of Applications

All of the applications above would be potentially feasible with the system that the team created. To prove this, the team had to characterize the system. This characterization is in terms of the efficiency, alignment time, and weight of the system in Chapter 3. The most important characteristic of the system is efficiency, as this needs to be enough for the system to reach the main requirement of causing tissue damage. Once the system was characterized, the relationship between the output power of the laser and the damage that was done on biological samples was

also assessed. These biological samples include cells as well as tissue. The study on cells aims to show that the laser is able to damage on a cellular level. The goal was to also show that the greater the power output, the greater the damage done. The cell study provides information about assessing how the laser affects a unit of cells together that make up a tissue. The team conducted a tissue study to further investigate how the laser can damage biological samples. The biological testing section uses pig ears, as these are the closest animal tissue to human skin. However, to prove the feasibility of these applications, the system damage must be present on both the cellular and tissue level as all the applications are so different.

Chapter 4: Results

This chapter encompasses all experimental results including the measurements and data referenced in previous chapters. The final design iteration of our system was used to collect biological testing results. A depiction of the final iteration can be seen in figure 41 below.
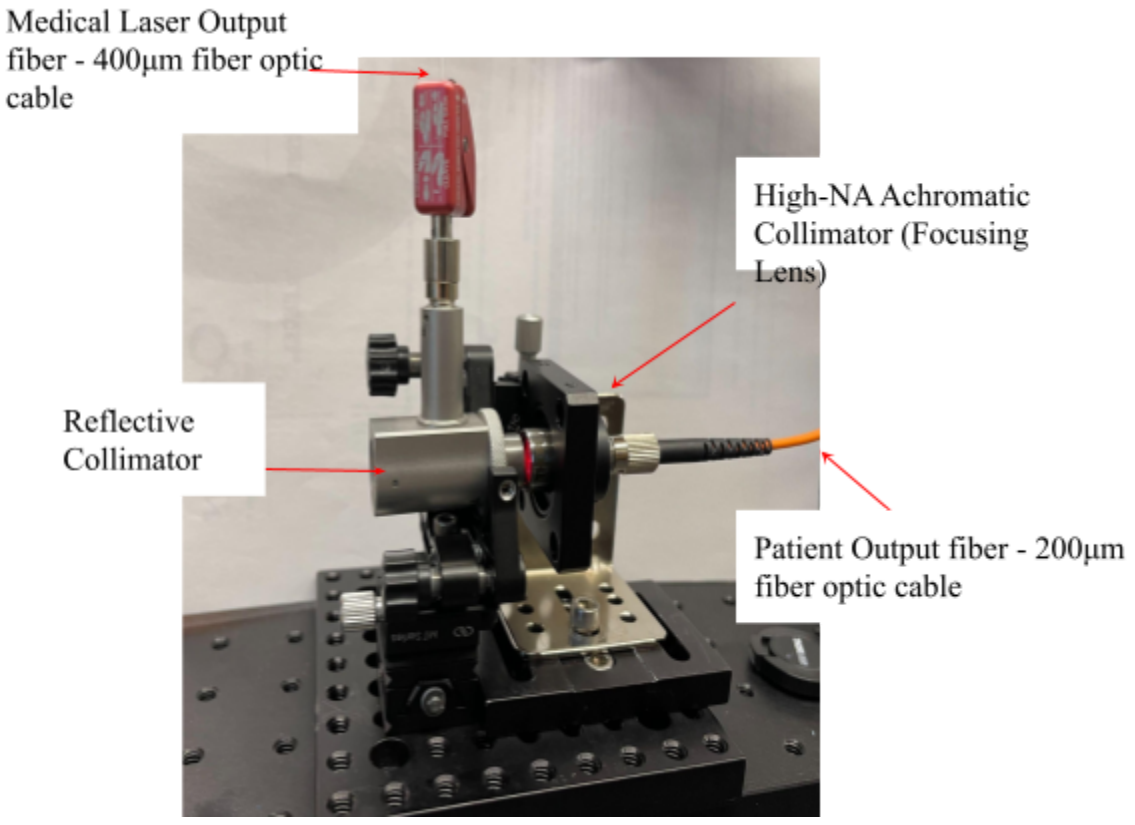
Figure 42: The optical fiber free-space coupling system setup depicting the fibers, collimators, and laser used.

4.1 Characterization of Optical Performance

The following subsection summarizes data obtained from optical performance testing with earlier design iterations. The data presented here also include some discussion and analysis.

Table 4-1-1: Testing prototype on design iteration 6: X-X Directional L-Stage Testing Results

Trial Number	Medical Fiber Output(W)	Patient Fiber Output(W)	Percentage(%)

1	0.78	0.16	20%
2	0.5(red)	0.25µW	0.05%

The result we got from the X-X directional stage design was not ideal due to the limitations we mentioned in the design iteration section. We first measured the medical fiber output, which is the input of the first collimator, and we measured the patient fiber output from the multimode fiber tip. A new sensor was obtained to better measure the intensity of the laser. This thermal sensor was better equipped for green light. Red light intensity was measured with a different sensor. Because different sensors were used for green and red light.

Table 4-1-2: Testing prototype on design iteration 6: X-Y Directional L-Stage Testing Results

Trial Number	Medical Fiber Output (W)	Patient Fiber Output (W)	Percentage (%)
1	0.77	0.13	16.8%
2	0.7	0.19	27.2%
3	0.485mW(red)	79.6µW	16.4%
4	0.457mW(red)	63.4µW	13.8%
5	0.460mW(red)	0.146mW	37.3%

After we improve the limitations mentioned in Chapter 2 including wobbling of the stage, we find out the efficiency increased 20.9%, especially for the red light. We used red light to align the system until it obtained the best efficiency result and then switched to the green light to continue alignment. We noticed that the alignment setup for the red light and green light do not produce the same efficiency. Aligning the system with green light on for a prolonged amount of time causes burning on both end faces of the fiber tips. The burning affects the transmission efficiency.

Table 4-1-3: Design iteration 11: Z-directional L-stage Testing prototype iteration II – Metal Stage Fabrication Results

Trial Number	Medical Fiber Output (W)	Patient Fiber Output (W)	Percentage (%)
1	0.48mW(red)	79.8µW	17%
2	0.48mW(red)	86.9µW	18%
3	0.47mW(red)	86.2 µW	18%

The testing from the fixed position on the metal stage did not result in great efficiency as we expected. This might be because although we obtained the most optimal efficiency position, other variables such as the angle between collimators might change, which affect the efficiency results. Then we changed the idea to fix position on the stage to add translational stages on the metal.

Table 4-1-4: Design iteration 11: Z-directional L-stage Testing prototype iteration II Results

Trial Number	Medical Fiber Output (W)	Patient Fiber Output (W)	Percentage (%)
1	0.48mW(red)	0.12mW	25%
2	0.51mW(red)	0.15mW	29%
3	0.50mW(red)	0.17mW	34%
4	0.50mW(red)	0.189mW	37.8%

The testing results from the Z-direction design iteration II increased nearly 10% from the previous setup. We changed the width of both plates to hold collimators. This data reflects the importance of the stability of the system. We focused on testing the red light efficiency and achieved a maximum of 37.8% transmission efficiency.

Table 4-1-5: Design iteration 12: X-Y-Z-directional L-stage Testing Prototype Results

Trial Number	Medical Fiber Output (W)	Patient Fiber Output (W)	Percentage (%)
1	0.45mW(red)	0.172mW	38.2%
2	0.64mW	0.126W	19.6%
3	0.64mW	0.133W	20.7%
4	0.64mW	0.14W	22.5%
5	0.64mW	0.15W	23.4%
6	0.46mW(red)	0.179mW	39.8%
7	0.46mW(red)	0.19mW	42.22%

The testing result from X-Y-Z directional L-stage testing design iteration II shows the best result we got through the term. We got a maximum of 42.22% transmission efficiency for red light and a maximum of 23.4% for green light. Due to the stability feature for metal boards in the

prototype, we get a chance to perform fine alignment in all x,y, and z directions. We aim to get better transmission efficiency when we test the new collimator on this setup in the next term.

4.2 Characterization of Laser-Tissue Interaction

After determining the final iteration of our coupling system, we characterized the damage our new setup could cause on biological tissue samples to demonstrate clinical potential. We also were interested in understanding the dependence of laser induced damage on the laser, as this relationship is fundamental to characterizing laser-tissue interactions. We procured pig ear, larynx, and trachea samples from Adams Slaughterhouse in Athol, Massachusetts. The samples are pictured (42) below.

42 (a)   42 (b)   42(c)
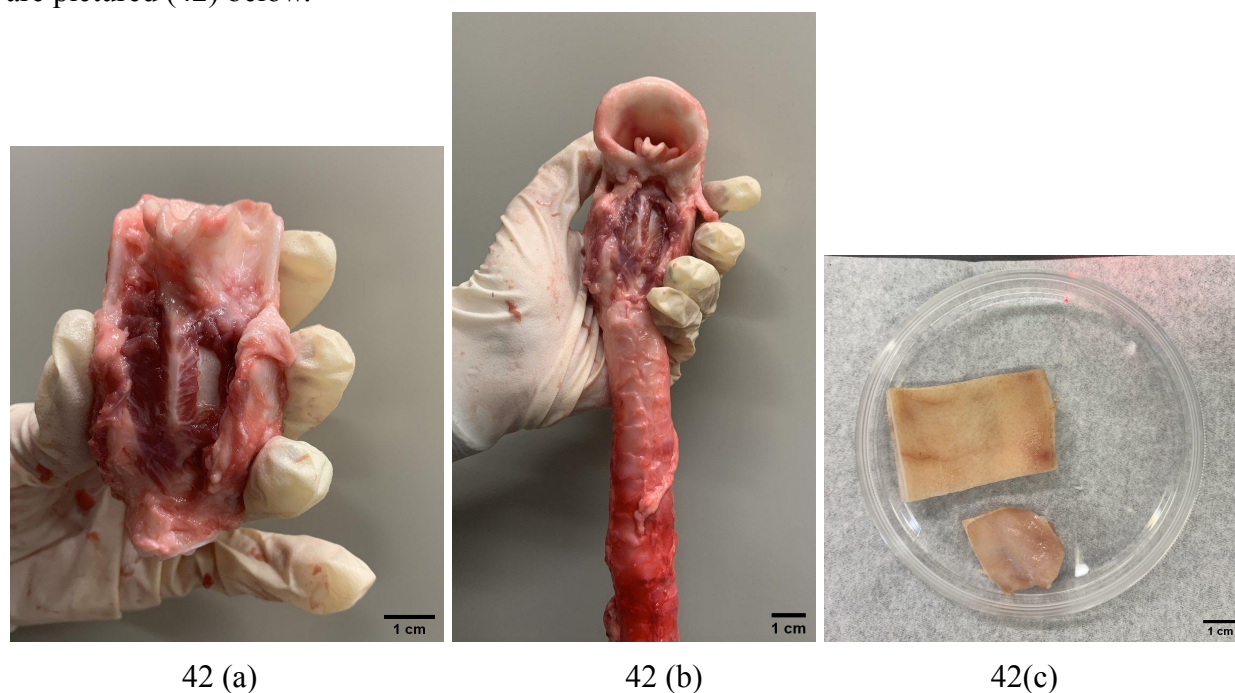
Figure 43: (a) Frontal display of larynx (b) Frontal display of larynx and esophagus(c) Pig ear sample

We then conducted a series of damage tests on these samples to simulate the damage that could be caused during surgical applications. Pictured below () is the testing setup we adhered to during biological experiments. This consisted of securing the multimode fiber and measuring its distance from the sample.
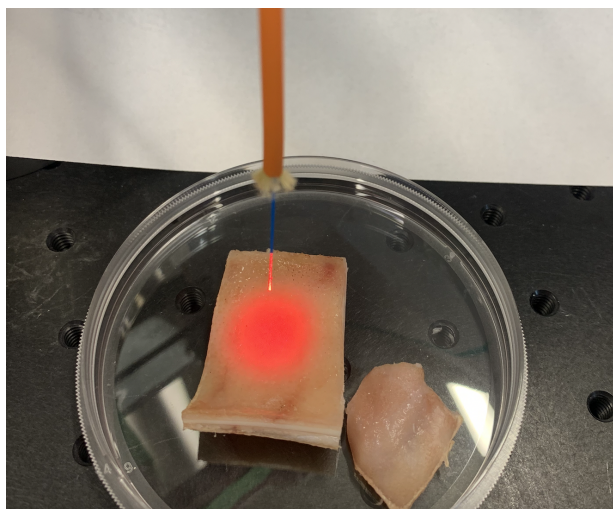
Figure 44: (a) Red light on pig ear set up   Figure 44: (b) Biological testing setup
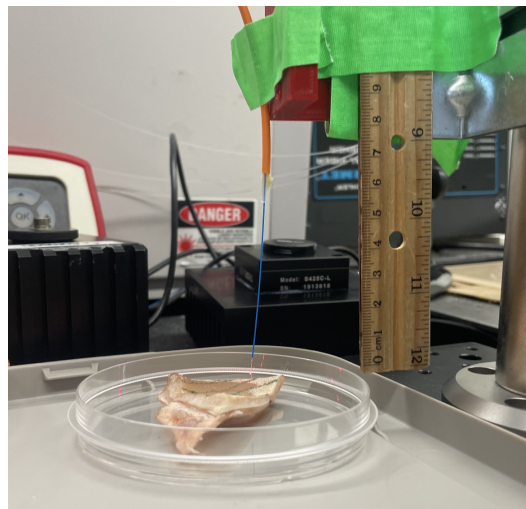
The damage tests and results desired were categorized by biological sample type. The pig ear samples were used to determine the initial parameters for biological testing. The setup included the use of either pig ears, larynx, or trachea samples. The pig ear tests were conducted after they have been defrosted and prepared according to the Biological Preparation Protocols found in Appendix 3. We first began baseline testing to understand how much energy is needed to make damage on the pig ears. The same baseline testing was conducted on the larynx and esophagus. Due to the difference in tissue biomechanics and tissue properties, a different baseline was determined for the different sample types. Using the baseline tests, we conducted further experiments to get a relationship between the depth of damage acquired and the time the laser light was held on the sample.

The first damage characterization experiment included determining the depth of damage caused by the system when pulse duration (τ), watts (W), rest interval (R), and height from sample (h) stayed constant while total laser exposure time (t) was varied. Three separate larynx samples were studied, and three trails for each time interval were conducted. A table depicting this data can be found in table 4.2.1 below.

Table 4.2.1: Larynx testing damage data, where $\tau 1$ is 1 second, W1 is 10 watts, and R is 0.2 seconds.

Larynx Damage Testing							
Sample	τ (s)	Watts (W)	T (time)	Rest Interval (s)	Depth of Damage 1 (um)	Depth of Damage 2 (um)	Depth of Damage 3 (um)
Larynx #1 Half #1	$\tau 1$	W1	2	R	365.26	483.97	454.93
Larynx #1 Half #1	$\tau 1$	W1	4	R	553.68	652.76	601.49
Larynx #1	$\tau 1$	W1	6	R	706.56	868.82	602.4

Half #1							
Larynx #1 Half #1	τ1	W1	8	R	889.65	901.11	876.45
Larynx #1 Half #1	τ1	W1	10	R	1207.52	1304.56	1256.63
Larynx #1 Half #2	τ1	W1	2	R	353.45	456.28	406.23
Larynx #1 Half #2	τ1	W1	4	R	929.93	1286.8	1348.56
Larynx #1 Half #2	τ1	W1	6	R	870.87	1110.22	947.93
Larynx #1 Half #2	τ1	W1	8	R	1172.94	1928.21	1546.78
Larynx #1 Half #2	τ1	W1	10	R	1369.75	1567.34	1426.89
Larynx #2 Half #1	τ1	W1	2	R	567.34	534.68	527.57
Larynx #2 Half #1	τ1	W1	4	R	908.56	863.58	905.69
Larynx #2 Half #1	τ1	W1	6	R	1023.71	1037.47	995.87
Larynx #2 Half #1	τ1	W1	8	R	1378.98	1467.83	1396.35
Larynx #2 Half #1	τ1	W1	10	R	1592.39	1546.47	1606.98

The damage depths found above (table 4.2.1) were calculated via a Keyence vhx-7000 series digital microscope. An example depiction of this calculation can be seen in figure __ below.
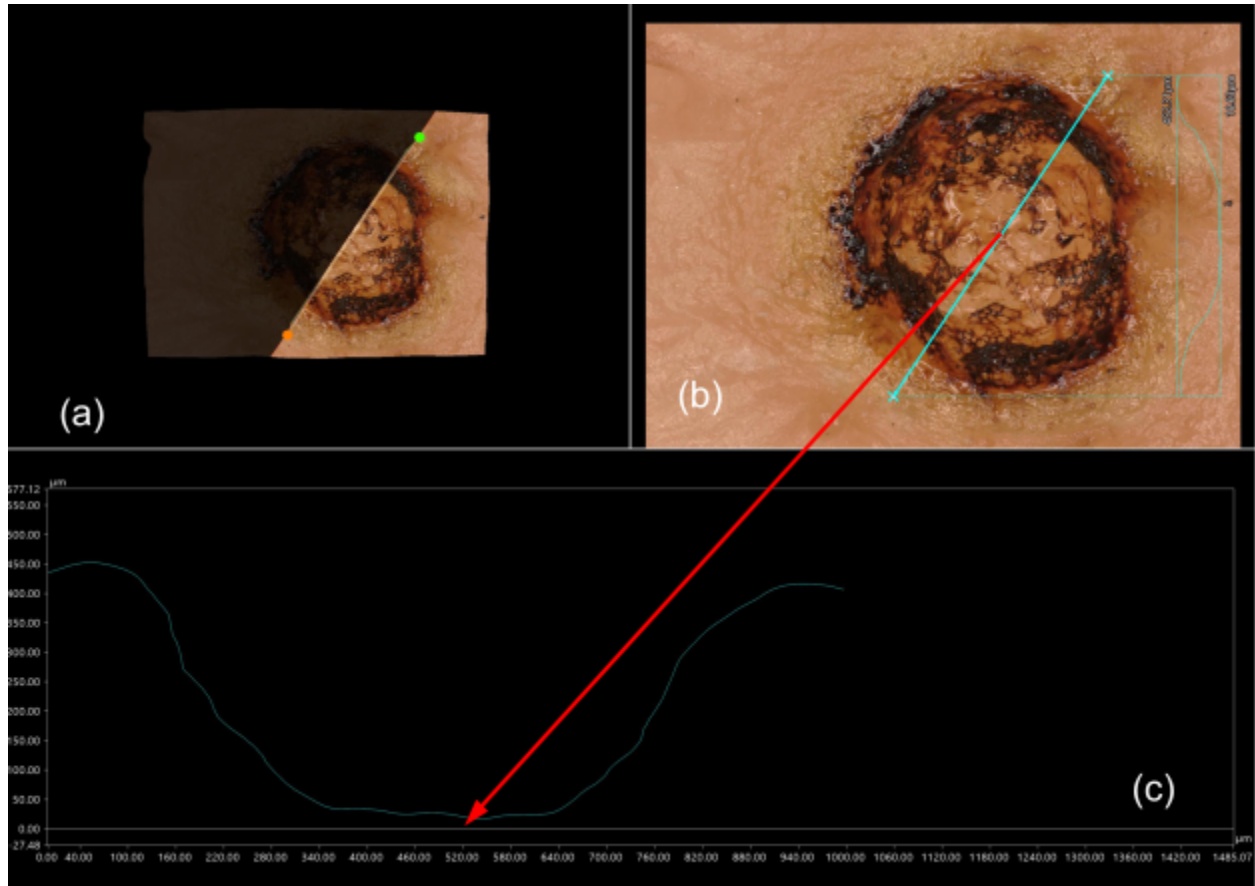
Figure 45: The Keyence vhx-7000 series digital microscope used allowed for the calculation of damage depth as seen above. Picture A in the figure shows an image of the burn as well as where the depth measurement is taken. Picture B also shows this. Picture C gives a graphical representation of the vertical high of the burn vs. the length of the burn. The dip in the graph corresponds to the distance (in µm) from the surface of the sample to the lowest point in the hole. The red arrow above points where the graph correlates to the image of the sample.

After determining the depth of damage after varying total laser exposure times, the damage was analyzed in comparison to the energy output (power, Ws) and the time of exposure. The graphs depicting these results can be seen in figures 42 and 43 below.
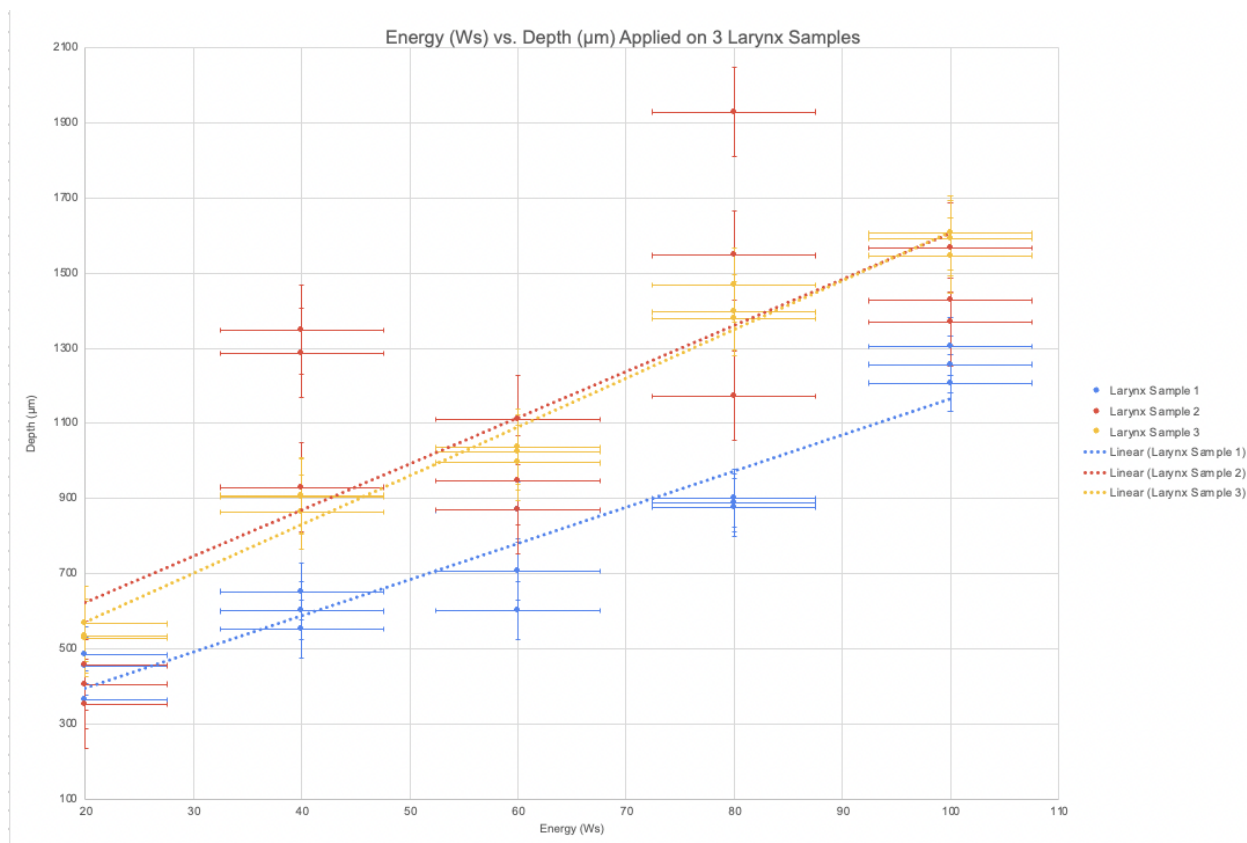
Figure 46: A graph of Energy vs. Depth of damage to a larynx sample. This data expresses the relationship between energy into a system and the damage it causes. A positive relationship between these variables can be seen.
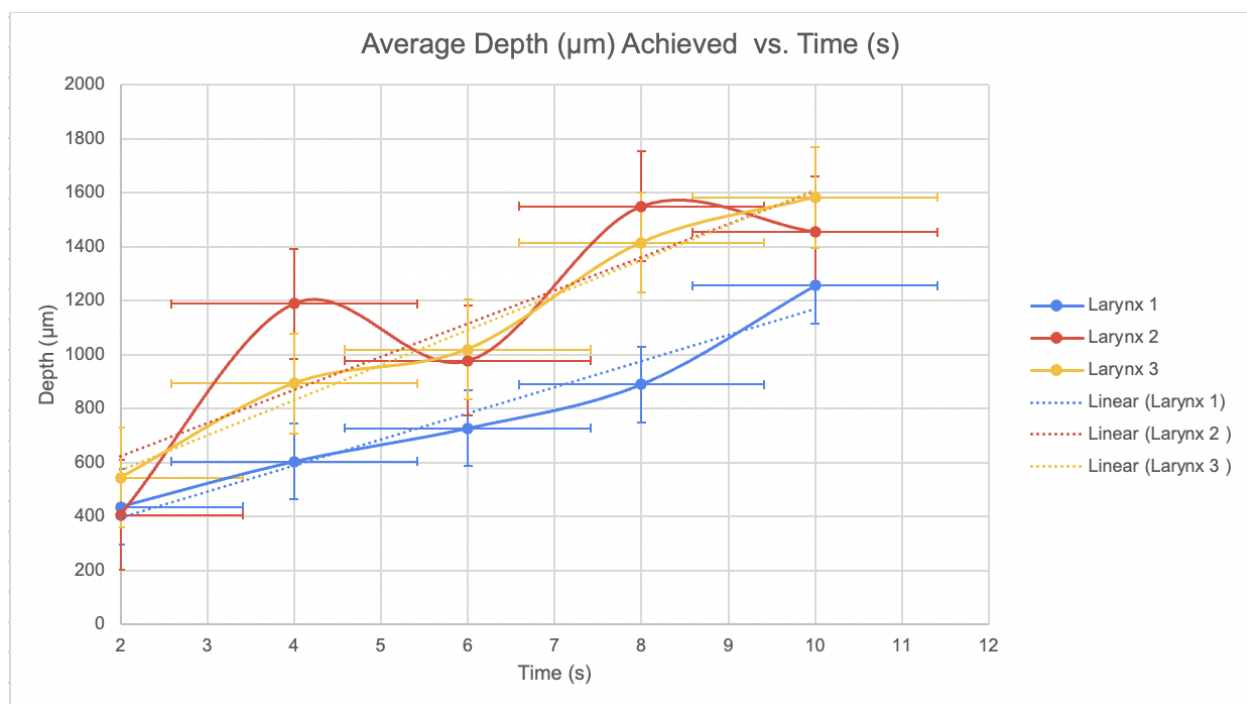
Figure 47: This graph contains the same data as the one above, but is able to show trend lines for each sample. There is a linear and non-linear trend line offered for each sample.

4.3 Characterization of Laser-Cell Interaction

After conducting the tissue study, the group further characterized the damage of this laser system by investigating the relationship between the laser and cells. This approach takes a more microscopic look at the damage done from the energy of the laser. This is important because the damage on a whole system, in this case the tissue, cannot be fully understood until the damage on all of its parts, the cells, can be characterized. Characterization of cellular damage from the laser can better inform the team on how that translates to damage to tissue. Before the experiment was conducted, the efficiency of the laser coupling system was characterized with the use of a power sensor and a power sensor head. 532 nm green light was passed though the endostat fiber and into the sensor head to produce a power reading of 0.72W, which was the power before our coupling system. The coupling system was set up and the smaller patient fiber was inserted into the power sensor head with the same green light. This produced a power reading of 0.33W, putting the efficiency of the system at around 46%. The control used was a plate of cells that were not affected by the laser. These cells were analyzed at the same time of the other plates and showed minimal variation in cellular attachment to the plate.

This experiment was conducted via the protocol found in Appendix 4 titled "Cell-Laser Testing Protocol". The cells used in this experiment were C2C12 cells. C2C12 cells are skeletal muscle found in mice. These cells were chosen for their rapid ability to proliferate, their availability, and their ability to show key morphological changes to distinguish between alive and dead cells [35]. This excerpt provided data on how many cells are left on the plate after cell damage vs. before. The use of different amounts of energy going into the system, the laser being held 1 mm away from the cells for different amounts of time, allows for the investigation of the relationship between cell damage and energy. This experiment is also able to show the morphological changes that happen to the cells after exposure to the laser. The results from the protocol followed are given below:
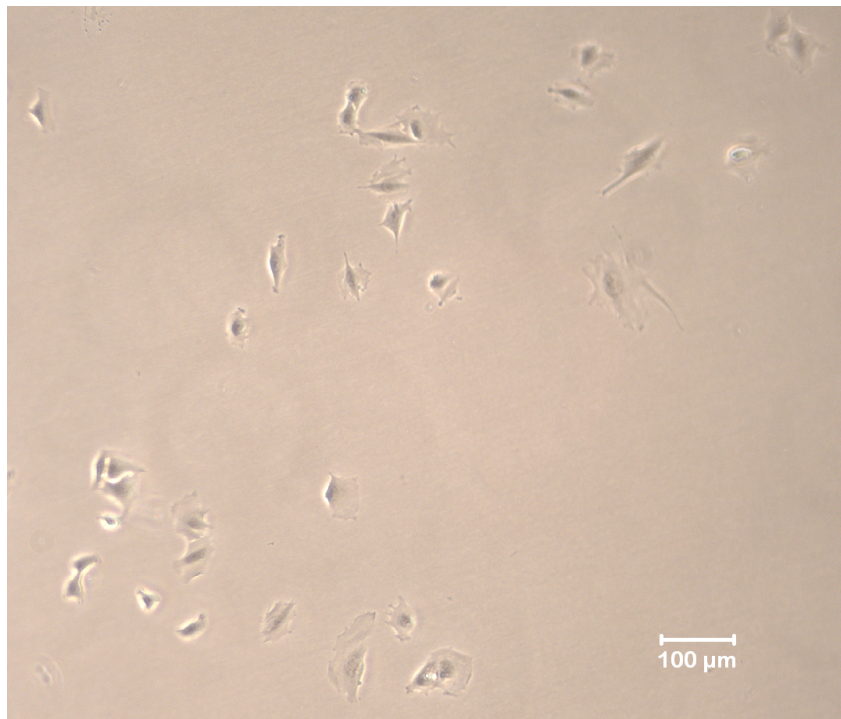
Figure 48: shows the C2C12 cells seeded on the cell plate before being exposed to the laser
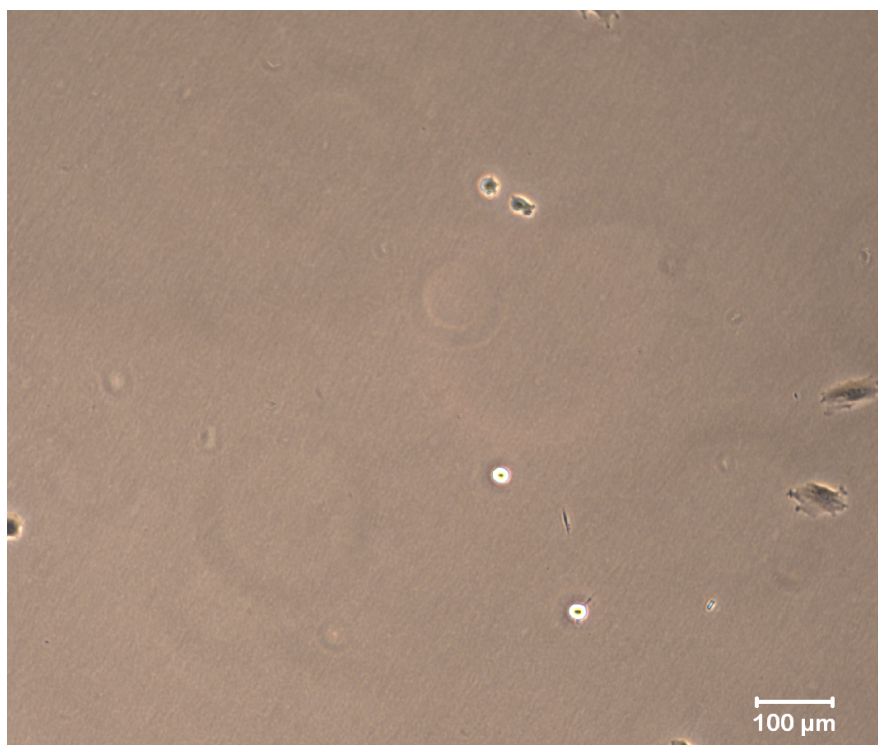
Figure 49: shows the C2C12 cells seeded on the cell plate after being exposed to 10 seconds of active 532nm green light from the laser system.

Figure 49 above serves as the control for the experiment. Here, the cells are seen before they have been exposed to the laser at all. Figure 48 shows how the cells look after exposure to the laser for 10 seconds. There is an apparent difference in the amount of cells attached to the plate as well as the amount of alive cells. The cells were also exposed to the laser at time intervals between 0 and 10 seconds. The results of that can be found below.

Table 4-3-1: Percentage of cells present after laser exposure as well as how long the cells were exposed to the laser.

Time of Active Laser of Cells (s)	Percentage of Cells Present After Laser	Standard Deviation
2	48.9%	+/-3.5%
4	52.8%	+/-2.6%
6	53.3%	+/-3.1%
8	64.3%	+/-2.6%
10	70.8%	+/-2.09%

This data can be plotted to better see the relationship between the time that the laser is actively shining on the cells, and the percentage of cells that are left on the plate after the laser is used. The graph of that data can be found below.
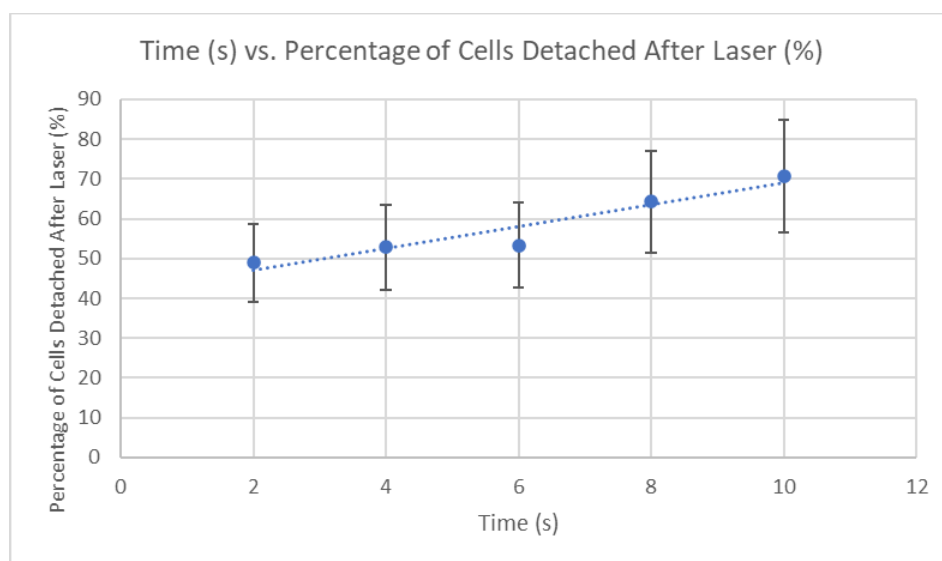
Figure 50: the graph of time in seconds vs. the percentage of cells detached after the laser exposure. The trendline is revealing a positive relationship between the two variables. Error bars were inserted as well, each time point came with three trials.

The graph above is able to visualize the data in a way where the relationship between the two variables can be observed. As mentioned in the introduction, the change in cell morphology was also observed by the group. The images below will serve to show that.
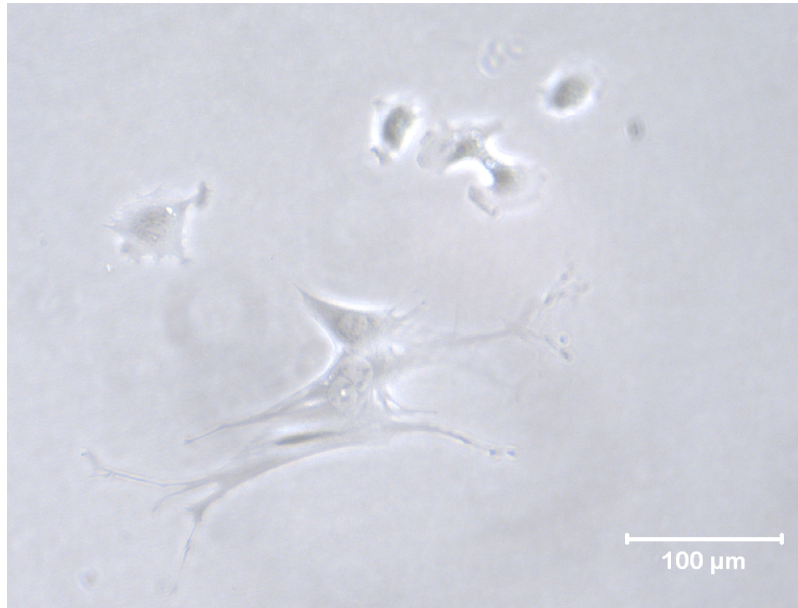
Figure 51: An image of healthy cells before exposure to the laser. The image was taken at 20X. The nucleus can be seen at the center of the cells. In addition, the cells are spread out as they are anchoring themselves to the plate and trying to reach out to make connections to other cells.
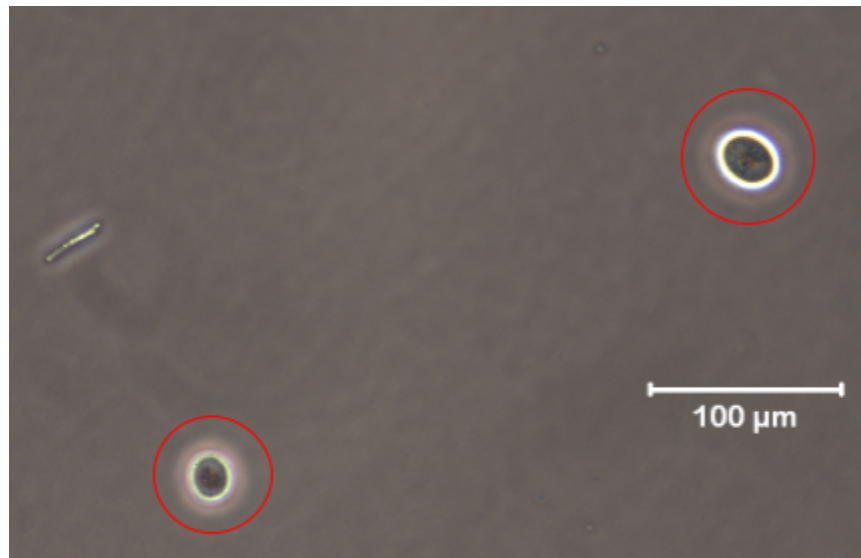
Figure 52: Cells after laser exposure for 10 seconds. These cells (circled in red) are dead and not attached to the plate. The cells were imaged away from the glass surface because they were detached. This can be seen as the cells are rounded and very dark in the center.

4.4 Larynx Model

A 3D larynx model was fabricated to help assist the mechanical team of this project. This was done using SOLIDWORKS and Rhinoceros. The mold was used for testing the efficiency of the laser in conjunction with the mechanical steerable portion. Below (figure 34) are images taken from different perspectives of the models created.

(a)   (b)   (c)
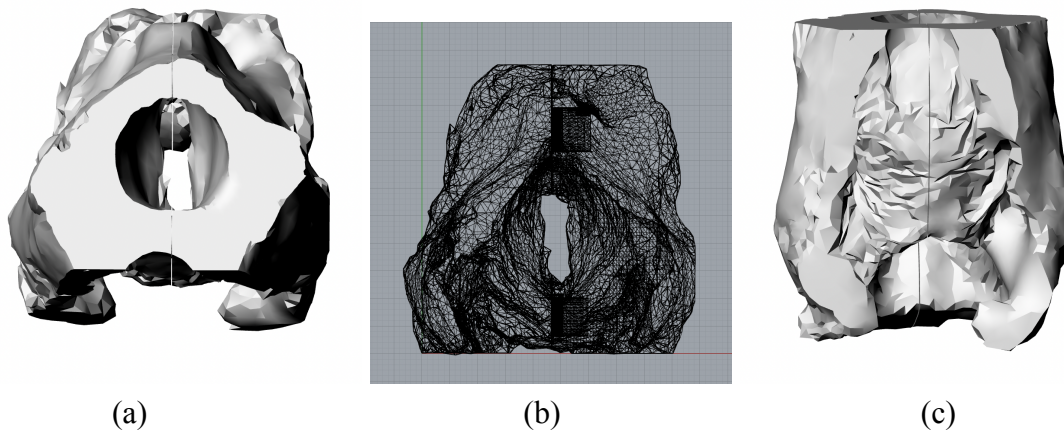
Figure 53 (a): Top view (b): Bottom view (c): Front view

While we aimed to fabricate this model using 3D printing, we determined that this could not be accomplished due to the lack of precision 3D printing offers, and because of the complex structure. The model was developed using an agarose gel in the printed mold. The model was developed to help the mechanical team conduct testing on the steerable portion to improve reachability and ease of manipulation of the system. There is no testing result available when the report is submitted.

4.5 Summary of the Capabilities and Potential for the Developed Laser Surgical System with Biological Samples

The motivation behind obtaining these results is verifying that we have developed a laser system capable of surgical application. The laser-cell interaction data is capable of showing the damage the laser system can do on a cellular level. In the results before this, the design was going through a verification process to ensure that the laser system fell within specifications that were appropriate for clinical application. Most of which were met. The experiment involving the laser-cell interaction works to validate that the system is able to, in the end, induce tissue damage. This damage is essential for all the possible applications of this system in terms of surgical use. The laser-tissue interaction data further validate the ability of the system to create significant damage on biological tissue.

With the characterization and verification of the device design, as well as the validation that the device is able to induce damage on biological samples, the surgical potential of this system can be realized. Surgical applications are discussed in Chapter 3 above. Above all, these experiments

were able to prove the potential for this device in surgery as it is able to damage tissue, a mode of damage that was able to be characterized with the chosen tissue.

Chapter 5: Discussion

5.1 Mechanical System Performance

While working through our design iterations we found that the size of the entire system plays a role in the efficiency and stability of the system. At the beginning of the project, we were thinking of reducing the size and weight by replacing the components of the system. In the initial design prototype, there are six heavy pieces in order to make fine alignment and keep the system robust. We tried to reduce at least one direction of those heavy translational stages. We started to test which direction of alignments affects the total power transmission efficiency the most by fabricating prototypes. The results did not show any great increase in terms of the total power transmission efficiency. The results indicated all direction alignments are important. We decided to try with miniature translational stages although that did not come with fine adjustment. With all degrees of freedom, the system showed an increase of 20% compared with single direction alignments. By grounding the system and eliminating the poles that were present in the earlier designs we were able to increase the stability of the system which increased the efficiency. As mentioned in the previous chapters, design with supporting poles will cause some extra problems to the system including the wobbling issue because of the great length of poles or heavyweight of optical parts.

Major achievements

Material:
In the final system setup, in order to increase the robustness of the entire system, we chose aluminum as the material for each part of the system and maintain a relative lightweight compared to other types of metal. This choice also prevents the system from breaking or deformation even in an ever-changing clinical environment.

Size:
The initial system setup was bulky, hard to carry, and wasted space. The design of the final system setup specifically worked to combat these issues. Throughout the design process, the system size decreased from 16 inches to 5 inches. The final smaller design can be carried easily and has more potential for clinical application.

Efficiency:
The power transmission efficiency of the final system is constantly around 53%, which is increased 13% from the initial system setup. The higher power transmission efficiency will reduce the time of the surgery operation compared to a lower power transmission efficiency system, which will increase the fiber tip damage cycle of both the endostat fiber and patient fiber.

Alignment time:
During the design process, we considered the alignment time. Alignment time includes the time it takes to align the two collimators and reduce the height differences between them in order to

increase the power transmission efficiency. The alignment time determines how much time is needed to prepare the system for clinical use. A short alignment time is needed, the less time it takes to prepare the system, the more practical it is for clinical use.

In the initial design, the approximate alignment time to achieve the average power transmission efficiency was 15 minutes. But if we want to achieve the best power transmission efficiency, some fine alignment is needed and will increase the total alignment time to 25 minutes or even longer. In the final design, the alignment time was reduced drastically, from 25 minutes to 10 minutes to achieve the best power transmission efficiency. This lower efficiency time was aided by the choice of all metal parts to prevent the system from wobbling and tilting. This improvement increased the feasibility and makes it more practical to bring the system into the operation room.

5.2 Optical Components Optimization

For the collimator selection, although we analyzed each key parameter of the collimators mentioned in Chapter 2 and ensured each collimator has the best match with the corresponding optical fiber, the total power transmission efficiency did not show better results. There are several aspects that could cause the result including defect of the collimator and size reduction of the outcome beam diameter. At first, we could not find what factor may cause the large power loss after the input collimator. Eventually we found that a piece of broken glass was blocking the laser transmission and causing the power loss. After we exchanged the broken collimator, we kept recording power output after each collimator and fiber. The data showed a large power loss after connecting the output patient fiber. Our guess is the size of the output beam diameter decreased from 8.5mm to 2mm, which may make it harder to align with the 200μm output patient fiber. So, the previous coupling system collimators were used for final testing.

We also noticed the fiber tip damage is another key factor that affects the overall power transmission efficiency. We usually polish the fiber tip after using green light every 3 or 4 times. At first we polished only one end of the patient output fiber that connects with the output collimator. Sometimes even if we polished that endface carefully, we noticed the power transmission efficiency is still not ideal. After several experiments, we found the other end of the patient output fiber also needs polishing. We performed the biological test with larger laser energy input and that caused a short fiber tip damage cycle. But after polishing or cutting both endface of the fiber, the overall power transmission efficiency will stay in a reasonable range that will not affect the accuracy of the testing results.

The size of the fiber plays an important role in the system. It not only determines the bending radius but also indicates how much light can be transferred from the collimator to the optical fiber. The initial and current size of the output fiber is 200 μm; we also tried with the 150 μm fiber. The result showed there was nearly no energy that could be transferred to the 150 μm fiber. The proper guess is the collimator outputs a relatively large diameter beam but only around 1 percent can be accepted by the 150 μm fiber. This result also made us decide to continue our testing with the 200 μm multimode fiber.

5.3 Biological Tissue Damage

The biological tissue damage testing proved that the laser system is able to cause damage to biological samples. The data gathered from the larynx testing presented in Chapter 4 portrayed an almost linear monotonic relationship between the energy (Ws) and depth of damage (μm). This positive linear relationship shows the direct dependence of the amount of energy put into the system on the damage it causes. The average depth achieved for each exposure time is as follows: 2 seconds caused 461.08 μm of damage, 4 seconds caused 670.92 μm of damage, 6 seconds caused 907.09 μm of damage, 8 seconds cause 1284.26 μm of damage, and 10 seconds caused 1430.95 μm of damage. We found that the depth increases by about 200 μm with every 2 seconds of applied laser light. The depth values allows a clinician to estimate how long they need to hold the laser on a lesion depending on the lesion dimensions.

This relationship between the energy and damage was expected because these results were obtained by Professor Loris Fichera in his work: *Cognitive Supervision for Robot-Assisted Minimally Invasive Laser Surgery* [36]. In this work, Professor Fichera showed that laser incision depth is a function of total laser exposure time. This relationship was characterized with a simple linear regression model similar to the one utilized in this report.

The results of larynx samples 1 and 3 most closely expressed a linear monotonic relationship. The two samples mainly differed in the overall magnitude of damage depth that was achieved. This could be due to intrinsic differences between the biological samples that would require one to need more energy than the other to get the same amount of damage. This is most likely caused by the fact that larynx 1 was less defrosted than larynx 2 and 3. Moreover, the larynx 2 sample did produce some outliers that did not fit into the linear, monotonic trend, and the depth of damage caused on larynx 1 was approximately 25% lower than the other sample's depth of damage. This may be due to the fact that the larynx samples are different pieces of biological tissue that intrinsically have differing mechanical and material properties. To determine if the timing between tests had any affect on the data, one could ensure that the testing intervals were even, and that the laser was given enough time to perform consistently at maximum efficiency after each sample. In the future, to discover if this could have caused the discrepancy in the data, one could characterize the biomechanical properties (strength, hardness, ductility) of the sample to determine if this plays a role in the discrepancy of laser damage.

The data collected by Professor Fichera not only portrayed this linear relationship, but his results conveyed that as energy continues to increase, the curve will eventually plateau [36]. The reason for this plateau is due to the thermal properties of the tissue. These properties determine how heat can dissipate through tissue. It should be noted that in both works, a pulsed laser was used. With a pulsing laser, the heat is able to dissipate into the tissue while the laser is off. Diffusion of heat into the surrounding tissue is necessary to achieve evenly burned tissue [37]. Tissue burned with a continuous laser creates a burning pattern that is not conducive to an even burn. Topographical evaluation and comparison of the burns made at different laser settings proves these conclusions. At a certain point, the energy dissipating out of the system becomes equal with the energy entering the system, and a plateau on the curve can be seen. This can also be due to charred tissue blocking the light from hitting other parts of tissue.

The data portrayed in this report did not produce an energy plateau. This could be because not enough energy was put into the system to observe the plateau of damage depth. This could also be due to the amount of data points taken, as more data points could more accurately represent a plateau in the curve. These data points were also not at a high enough energy to see this trend. Effort to include these data points can be built upon in future work.

5.4 Cell-Laser Damage Test

The cell-laser damage test allowed the team to better understand the impact the laser has on biological samples. In order to characterize damage on the system, the damage of each part should be assessed. This cell study was able to investigate the relationship between cell damage and the energy the laser system puts out. The more time that the laser was held on the sample, it seemed that the more damage was observed. In this study, damage was quantified in terms of the amount of cells that detached from the plate in relation to before vs. after exposure to the laser. This exposure was done at time points 0, 2, 4 6, 8 and 10 seconds. The reason why this metric was used to quantify cell damage is that damaged cells appeared more round and either stayed on the plate, or became detached and floated off in the media [39]. The number of cells present on the plate that were alive was a good metric for assessing which cells were left undamaged enough vs, which well were completely damaged by the laser. Figures 44, 45, 47 and 48 show how the laser is about to change the morphology of the cells. Mechanisms for cell death/damage from lasers have been explored by recent articles, like one written by James O'Connor [37]. O'Connor describes the mechanism as one that "involves a combination of photochemical, photothermal, and photomechanical effects," [37]. Authors of this article also have found that the presence of damaged cells that are still alive after exposure to the laser, can be beneficial in recruiting important factors for healing [38].

Figure 46 is a graphical representation of the relationshiship that the laser has on the cells. Specifically, it depicts the relationship between the time the laser is held on the sample and the percentage of cells that are left attached to the plate after the laser exposure. The reason for this quantification of damage is described in the paragraph above. This graph was able to produce a positive relationshi between the number of cells that detach from the plate and the amount of energy that is put into the system. The cell plate that was exposed to the laser for the longest had the highest percentage of detachment whereas the plate with the least amount of laser exposure had the smallest percent of detachment. Statistical analysis was done to produce the error bars on the graph. Error was a bit high, but this could be due to a variety of factors. The first is that the cells had to be moved around quite a bit to capture images and conduct the experiment. Ideally, the plate would not be moved around so much as to prevent premature detachment of the cells. This could lead to a higher amount of cell detachment recorded than is actually happening. The next source of potential error is that the cells were not allowed to proliferate to full confluency. Allowing the cells to be fully confluent on the plate may allow for a more accurate analysis of cell detachment. Another source of error could be that there were not enough data points. More data points should be collected to further validate this possible positive relationship between energy into the system and damage to the system. Other modes of investigation can be done such

as using dyes that can indicate cell death. This may be able to better quantify the number of dead vs. alive cells in this study. It also may help in reducing error in the study.

This study was able to help the team further validate the damaging effect that the laser has on biological samples. The team can use this data to better understand the system, the tissue, by understanding the parts of the tissue, the cells. The team was able to begin to characterize this damage as well as validate that the laser system can do damage on a cellular level.

Chapter 6: Educational Outcomes and Reflections

6.1 Challenges in E2

Working with this system, the team identified challenges and gaps to overcome. The first major challenge faced was the size of the system. The initial setup was big and heavy making it not ideal for clinical use. The final design must be lightweight and sturdy so it can withstand minor drops and damage. Another major issue the team ran into is that end faces of multimode fiber tips are easily damaged by high laser power. The coupling efficiency will decline after 15-20 seconds due to end face photodamage [8]. The next issue deals with alignment time. Alignment is very important to achieving the proper efficiency of the coupling system. The time it takes to align the system however should be quick, especially for an outpatient procedure that does not require a lot of time. Doctors and medical staff will not want to take the time to realign the system. To address this, the system should be stable to eliminate the need for constant realignment. The final issue the team found is related to the mechanical team who has been working on creating a caging system to bend and rotate the fiber inside the patient. The mechanical team found that the fiber used was causing a deflection issue within their device. With the fiber inserted into the caging system, they were unable to achieve the same high degree of bending as when the fiber is not present.

6.2 Challenges in A term

The main challenges and realizations that were encountered throughout A-term were within the design loop and the 3D printed stages that were printed each week. The material used for the 3D printed stages was bendable plastic which resulted in lower efficiency values due to uncontrollable bending. Despite this drawback of the 3D printed stages, they helped us understand what design and alignment of the collimators would yield the highest efficiency and the most compact design. We also noticed that the collimators are very sensitive and no matter how secure the collimator stage is, the system is very delicate and any slight movement can significantly impact the efficiency. This is a challenge that we have not been able to solve yet, and hope to address it in our final metal stage.

6.3 Challenges in B term

There were two main challenges that were encountered throughout B term. The first is that the system performance was not consistent during biological sample testing. When conducting the biological sample testing, it was observed that the system showed varying performance in terms of efficiency and ability to burn. We determined that when the system had very low efficiencies on some trials, then polishing and realignment were required. The second main issue is that the new equipment that was ordered to improve the system came with a long lead time, a defect, and a need to troubleshoot these issues. As a result, the team did not have all the anticipated hardware for the system to optimize the efficiency of the system.

Chapter 7

7.1: Broader Impact

The implementation of this device requires consideration as to what effect this device could have on the world. This includes economic, environmental, sustainability, manufacturability, ethical, health and safety, social, and political considerations. Looking at this device from an economic standpoint, the device would have a relatively low cost, can be used many times, and would save the clinical and patient money compared to the current standard of care. This is due to the decrease in anesthesia, time in the hospital, recovery time, etc. Environmental and sustainability considerations are not very applicable to the device other than the fact that it is not single use, and does not require resources other than power. In terms of manufacturability, the system is simple to create, the most complex part of the system is the laser. A trusted medical laser company should be sourced for this. Another important consideration is the ethical consideration. Throughout our work, we ensured that all testing and protocols were ethically sound. The biological samples used in testing were ethically sourced from a USDA and research approved site. All protocols were written and carried out to ensure the safety and efficacy of our results. We believe that this work will have a positive impact on society, and improve the lives of patients in need of otherwise intense, invasive medical procedures. The next consideration is health and safety. The main focus of our work was to improve the implementation methods and results of common medical surgeries. Once completed, our coupling system has the potential to directly impact everyday medical patients in need of laryngeal throat surgery or other kinds of precise medical laser procedures. Our hope is that it will make common surgeries less dangerous for the patient to receive, and easier for the doctor to perform. We also hope to decrease the recovery time of applicable medical procedures which could contribute to creating a more productive, healthy society. In addition, safety protocols are used by the team as well as taught to anyone using the system to ensure safe use. Social and political considerations are not very applicable to this system. If anything, the clinicians and patients would prefer a better method to the current standard of care for surgeries that can benefit from this system.
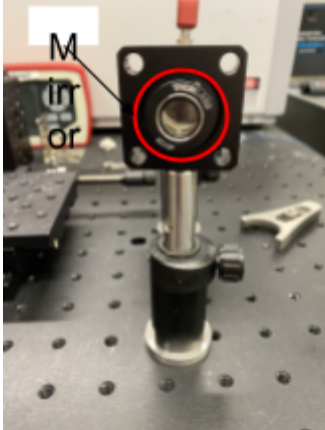
7.2 Conclusion and Outlook for Future Work

Throughout this project, the team was able to better the system and start to model the laser damage on biological samples. There is still work that needs to be done in the future to make this system ideal for clinical use. The first is that the efficiency can still be made better. This task is quite difficult as the laser is being used and the endostatin fiber has been discontinued. In addition, there's a large difference between the diameter of the endostat fiber and the diameter of the patient multimode fiber, making getting a high coupling efficiency difficult. Further changes in equipment can be investigated in the future to better the coupling efficiency of the system. One important change could be the use of a different laser entirely. More work that can be done in the future is further investigation into the effect of the laser on tissue. More data points with different types of tissues can further validate this process as well as expand the potential applications. In addition, more data can be collected on the effects of different pulsatile rates to

establish the best rate to use clinically for each application. This all especially needs to be done once the system is at a higher coupling efficiency. The last aspect of future work that can be done is more microscale investigations into how the laser affects the

tissue. Analysis at a microscopic level of cells exposed to the laser will help to quantify the laser damage. Overall, this system has a great potential to help a wide variety of patients and more data needs to be collected to support this.

Appendix

Appendix 1: Parts of the System of the First Iteration

Name of part	Diagram of part	Purpose
High-NA Achromatic Collimators for Multimode Fibers		This part is a mirror that helps to focus the light into the fiber. The motion that this lens focuses is in a digital plane.
X-axis translation stage		This part is to move the collimator in the +/- X direction for optimal alignment.(arrow is the direction of light)
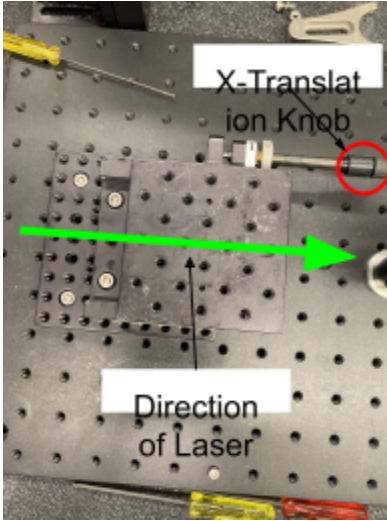
Y-axis translation stage	Y-Translation Knob Y-direction Direction of Laser	This part is to move the collimator in the +/- Y direction for optimal alignment
Z-axis translation stage	Direction of Laser Z-Translation Knob	This part is to move the collimator in the +/- Z direction for optimal alignment. (label)
Collimator	Fiber location	This part contains a small curved mirror. This mirror takes the light from the medical fiber optic cable and collimizes it.
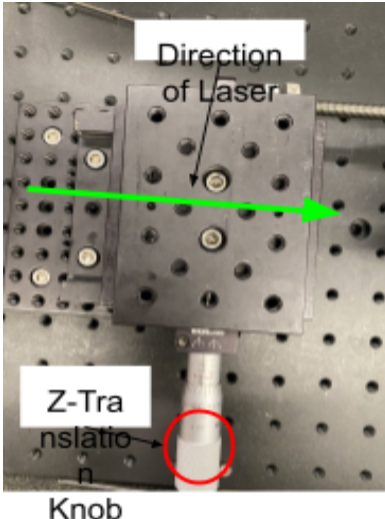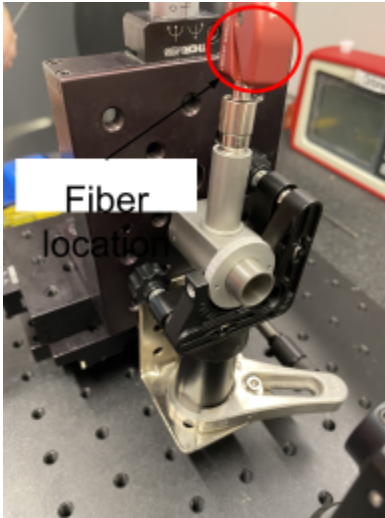
	Fiber Location	
Top view of system featuring the fiber optic terminator		This is the fiber optic terminator which is meant to hold the thicker medical optical fiber in place so that the laser can be collimated and focused into the smaller medical fiber.
New Setup		This is the new mechanical alignment setup for the coupling system.
Biological Testing Setup		This is the testing setup for the biological testing that is done.
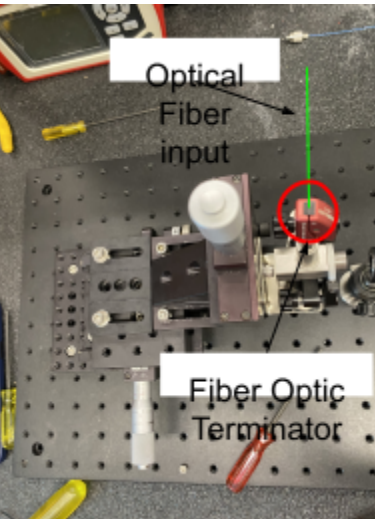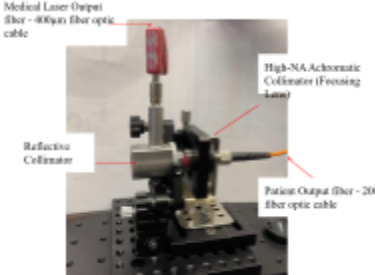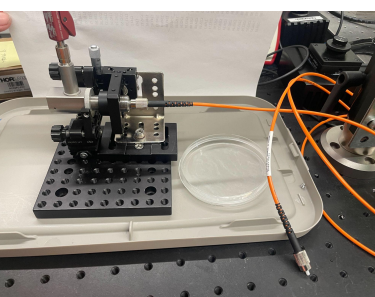
Appendix 2: Vocabulary

Term	Definition
Coupling Efficiency	The efficiency from the end of the endostat fiber to the end of the patient fiber
Endostat Fiber	The fiber leaving the laser and entering the first collimator
Patient Fiber	The fiber leaving the collimator and entering the patient
Thermal Damage	The damage that is induced by the light coming through the fiber optic cable
Overall Efficiency	Efficiency of the system from the laser to the end of the patient fiber
Collimator	A collimator is able to collimate and refocus light to and from fiber optic cables
Numerical Aperture	This number characterizes the angle of the light exiting a fiber optic cable

Appendix 3: Biological Sample Handling, Storage, and Preparation

Tissue Procurement and Storage:

Acquired pig ear samples from Adams slaughterhouse will be kept frozen until testing day. Time is an important factor with respect to sample degradation; therefore, it is necessary to minimize the time between the harvesting of the sample and properly preserving the sample [32]. Failure to preserve the sample in a timely manner exposes the sample to potential changes in cell morphology due to endogenous enzymatic degradation of analytes [32]. The first processing step is to snap-freeze the sample by exposing the tissue to a cryogen such as liquid nitrogen, liquid pentane, or hexane/dry ice. Generally, the tissue is placed in a loose foil wrapper and immersed in the cryogenic solution slowly to prevent fracturing the tissue. Care must be taken to avoid deformation of the tissue by the container. One useful technique is to fashion a float out of aluminum foil, place the tissue in the float on top of liquid nitrogen, allow the sample to freeze, then wrap and immerse the tissue fully. This technique causes the tissue to freeze more slowly than immediate immersion and can be useful for tissues such as the brain that are prone to

fracture during the freezing process. This technique also has the added advantage that the morphology is more readily preserved. Depending upon the importance of the sample orientation, it might be necessary to record or mark the specimen orientation before long term storage. Prior to testing the day the samples will be defrosted overnight to ensure their readiness for testing.

Tissue Storage and Preparation:
Upon receival of the samples, they will be drained of fluids, and washed with IPA. The larynx sample was dissected to remove muscular surroundings and cut the sample into desired sizes. The samples were then frozen and stored in petri dishes until further use. The samples were defrosted overnight under refrigeration the day before we plan on testing. The recommended cutting temperature for skin is -25°C.

Appendix 4: Biological Testing Protocols

Tissue-Laser Testing Protocol:

The biological sample can be acquired, stored, and prepared with the protocol found in appendix 3. At this point, everyone should have safety gear on. After this, the sample can be tested on. To do this, the sample can be drawn on with a sharpie to make a grid for testing. Each square can be subjected to a different power or pulse, that is up to those conducting the test based on what variable is being changed. The sample can be moved into a plastic containment unit to contain the fumes that will arise from testing. This box should be cleaned with IPA. Before the testing, the fibers in the system should be polished, and the highest coupling efficiency of the system should be reached. With this set, the testing can begin. The patient fiber should be held at a constant height above the sample, so it can be taped to an extra structure in a way that it is perpendicular with the sample. The fiber tip should be around 1-3mm from the sample, ideally 1 mm above. The laser settings can be changed based on what is being tested. The laser can then be aimed into the respective square using the red light. Once the team has the laser safety goggles on, the pedal can be pushed to activate the green light. The light will be applied for a predetermined time. All the tests can be conducted with the use of multiple trials. Once all the damage is done to the sample, it can be analyzed.

Tissue Testing Analysis:

Once the samples have been tested, the damage needs to be analyzed. This is done with the use of a Keyence microscope. This microscope is able to conduct a 3D model of the damage and allows for the quantification of the depth of the damage done by the laser. This data can then be compared to the amount of energy put into the sample to create a graphic display of the relationship between the energy used and the damage.

Cell-Laser Testing Protocol:

Proper PPE, such as a lab coat, gloves, and goggles should be worn, and materials should be gathered. Materials include: cell suspension, 6 cell plates, a micropipette, a hemocytometer, the laser coupling system, a laser, an endostat fiber, and a 200um fiber. The complete laser system can be put together using the coupling system, the laser, and the fibers. To prepare the samples, cells must be taken from a test tube with cells suspended in 5mL of media. Count the cells per mL with the use of a hemocytometer. Add 25,000-50,000 cells to each plate with enough media to cover the bottom, about 5-10mL. The cells can be added with a micropipette. Place the plates in an incubator and allow them to stick to the plate and proliferate, this will take 2-3 days. The incubator should be kept at 27°C with 5%CO2.

After the cells have proliferated, check them under a microscope to check for confluency. Take 3 photos of each plate at 10X, count how many cells are in each picture and record the number on a data sheet. Take the cells to the already set up laser system. The system should be warmed up and set up to the highest efficiency by utilizing alignment. The laser should be set up on the pulsed setting with a τ value of 1s and a rest interval, R, of 0.2 seconds. Plate 1 will serve as a control and will not be affected by the laser. Take plate 2 and expose 10 spots with the laser. The fiber should be held 1mm over the sample. The amount of active time that the laser should be on the sample is 2 second. This is to be repeated for plate 3, 4 and 5 but for 4, 6, and 8 seconds, respectively. After, take the plates to the microscope to image them. Find areas that the laser did damage. Take an image of three of those spots at 10X. Count the cells in each image and record in a data sheet. From this data sheet, the time that the laser was active on the sample in seconds can be related to the % of cells present before vs. after the laser. To clean up, the optical fiber should be cleaner with IPA. The cell plates can be disposed of properly in biohazard waste.

Appendix 4: Code - Motorized Stage

```
function motors_Callback(hObject, eventdata, handles)
global Ldevice Rdevice timeout

if get(handles.motors,'value') == 1

  %Load assemblies
  NET.addAssembly('C:\Program Files\Thorlabs\Kinesis\Thorlabs.MotionControl.DeviceManagerCLI.dll');
  NET.addAssembly('C:\Program Files\Thorlabs\Kinesis\Thorlabs.MotionControl.GenericMotorCLI.dll');
  NET.addAssembly('C:\Program Files\Thorlabs\Kinesis\Thorlabs.MotionControl.KCube.DCServoCLI.dll');

  %Initialize Device List
  import Thorlabs.MotionControl.DeviceManagerCLI.*
  import Thorlabs.MotionControl.GenericMotorCLI.*
  import Thorlabs.MotionControl.KCube.DCServoCLI.*

  %Initialize Device List
  DeviceManagerCLI.BuildDeviceList();
  DeviceManagerCLI.GetDeviceListSize();
```

```matlab
    %Should change the serial number below to the one being used.
    Lserial_num='27500725';
    Rserial_num='27256780';

    timeout=600000;

    %Set up device and configuration

    Ldevice = KCubeDCServo.CreateKCubeDCServo(Lserial_num);
    Ldevice.Connect(Lserial_num);
    Ldevice.WaitForSettingsInitialized(5000);

    Rdevice = KCubeDCServo.CreateKCubeDCServo(Rserial_num);
    Rdevice.Connect(Rserial_num);
    Rdevice.WaitForSettingsInitialized(5000);

    % configure the stage
    LmotorSettings = Ldevice.LoadMotorConfiguration(Lserial_num);
    RmotorSettings = Rdevice.LoadMotorConfiguration(Rserial_num);

    LmotorSettings.DeviceSettingsName = 'Z825';
    RmotorSettings.DeviceSettingsName = 'Z825';

    % update the RealToDeviceUnit converter
    LmotorSettings.UpdateCurrentConfiguration();
    RmotorSettings.UpdateCurrentConfiguration();

    % push the settings down to the device
    LMotorDeviceSettings = Ldevice.MotorDeviceSettings;
    Ldevice.SetSettings(LMotorDeviceSettings, true, false);

    RMotorDeviceSettings = Rdevice.MotorDeviceSettings;
    Rdevice.SetSettings(RMotorDeviceSettings, true, false);


    Lpos = System.Decimal.ToDouble(Ldevice.Position);
    set(handles.Lmotor_position,'string',num2str(Lpos))

    Rpos = System.Decimal.ToDouble(Rdevice.Position);
    set(handles.Rmotor_position,'string',num2str(Rpos))


    set(handles.motors,'string','Motors (Connected)')


else
    Ldevice.Disconnect()
    Rdevice.Disconnect()
    set(handles.motors,'string','Motors (Disconnected)')
end

function Lhome_Callback(hObject, eventdata, handles)
global Ldevice timeout Rdevice

set(handles.LmotorS,'string','Motor is "Moving"','ForegroundColor','r')
pause(0.0001)
Ldevice.Home(timeout);
pause(0.0001)
set(handles.LmotorS,'string','Motor is "Idle"','ForegroundColor','k')
```

```matlab
Lpos = System.Decimal.ToDouble(Ldevice.Position);
set(handles.Lmotor_position,'string',num2str(Lpos))

Rpos = System.Decimal.ToDouble(Rdevice.Position);
set(handles.stgdis,'string',num2str(-Lpos-Rpos+56,'%.2f'))

function Lstart_Callback(hObject, eventdata, handles)
global Ldevice timeout Rdevice

Lpos = System.Decimal.ToDouble(Ldevice.Position);
step = 26-Lpos-str2double(get(handles.tube,'string'))/2;
V=Ldevice.GetVelocityParams;
V.MaxVelocity=str2double(get(handles.velocity,'string'));
Ldevice.SetVelocityParams(V)
set(handles.LmotorS,'string','Motor is "Moving"','ForegroundColor','r')
pause(0.0001)
Ldevice.MoveTo(Lpos+step,timeout)
pause(0.0001)
set(handles.LmotorS,'string','Motor is "Idle"','ForegroundColor','k')

Lpos = System.Decimal.ToDouble(Ldevice.Position);
set(handles.Lmotor_position,'string',num2str(Lpos))

Rpos = System.Decimal.ToDouble(Rdevice.Position);
set(handles.stgdis,'string',num2str(-Lpos-Rpos+56,'%.2f'))

function Lbackward_Callback(hObject, eventdata, handles)
global Ldevice timeout Rdevice

Lpos = System.Decimal.ToDouble(Ldevice.Position);
step = str2double(get(handles.step_size,'string'));
V=Ldevice.GetVelocityParams;
V.MaxVelocity=str2double(get(handles.velocity,'string'));
Ldevice.SetVelocityParams(V)
set(handles.LmotorS,'string','Motor is "Moving"','ForegroundColor','r')
pause(0.0001)
Ldevice.MoveTo(Lpos-step,timeout)
pause(0.0001)
set(handles.LmotorS,'string','Motor is "Idle"','ForegroundColor','k')

Lpos = System.Decimal.ToDouble(Ldevice.Position);
set(handles.Lmotor_position,'string',num2str(Lpos))

Rpos = System.Decimal.ToDouble(Rdevice.Position);
set(handles.stgdis,'string',num2str(-Lpos-Rpos+56,'%.2f'))

pause(0.0001)
Rdevice.MoveTo(Rpos-step,timeout)
pause(0.0001)
set(handles.RmotorS,'string','Motor is "Idle"','ForegroundColor','k')

Rpos = System.Decimal.ToDouble(Rdevice.Position);
set(handles.Rmotor_position,'string',num2str(Rpos))

Lpos = System.Decimal.ToDouble(Ldevice.Position);
set(handles.stgdis,'string',num2str(-Lpos-Rpos+56,'%.2f'))
```

Bibliography

[1] J. H. Hah, S. Sim, S.-Y. An, M.-W. Sung, and H. G. Choi, "Evaluation of the prevalence of and factors associated with laryngeal diseases among the general population," The Laryngoscope, vol. 125, pp. 2536–2542, July 2015.

[2] M. Remacle and H. E. Eckel, Surgery of larynx and trachea. Springer, 2010.

[3] C. Y. Kuo and S. L. Halum, "Office-based laser surgery of the larynx: cost-effective treatment at the office's expense," Otolaryngology–Head and Neck Surgery, vol. 146, no. 5, pp. 769–773, 2012.

[4] C. J. Rees, G. N. Postma, and J. A. Koufman, "Cost savings of unsedated office-based laser surgery for laryngeal papillomas," Annals of Otology, Rhinology & Laryngology, vol. 116, no. 1, pp. 45–48, 2007.

[5] D. Stoeckel and A. Melzer, "The use of ni-ti alloys for surgical instruments," Materials in Clinical Applications, ed. by P. Vincenzini. Techna Srl, pp. 791–798, 1995.

[6] S.T.Liu, P.B,Abell, and S.Q.Johnson, "*Scream 3.0: Super-elastic Continuum Robot for Endoscopic Articulation and Manipulation".* : Worcester Polytechnic Institute, 2021.

[7] M. Runciman, A. Darzi, and G. P. Mylonas, "Soft Robotics in Minimally Invasive Surgery," Soft Robot, vol. 6, no. 4, pp. 423–443,2019.

[8] M.Zhu, Y.Shen, A. J. Chiluisa, J.Song, L.Fichera, and Y. Liu"Optical Fiber Coupling System for Steerable Endoscopic Instruments" in Medicine and Biology Conference, IEEE Engineering in Medicine and Biology Society,May,2021

[9] Goldberg, J. (2020). *Laser vocal cord surgery*. Laser Vocal Cord Surgery | Jeffrey E. Goldberg, MD. Retrieved January 30, 2022, from https://www.jgoldbergmd.com/laser-vocal-cord-surgery.php

[10] Passi, D., Pal, U. S., Mohammad, S., Singh, R. K., Mehrotra, D., Singh, G., Kumar, M., Chellappa, A. A., & Gupta, C. (2013). Laser vs bur for bone cutting in impacted mandibular third molar surgery: A randomized controlled trial. *Journal of oral biology and craniofacial research*, *3*(2), 57–62. https://doi.org/10.1016/j.jobcr.2013.03.006

[11] Chan, A. Y., Tran, D. K. T., Gill, A. S., Hsu, F. P. K., & Vadera, S. (2016). Stereotactic robot-assisted MRI-guided laser thermal ablation of radiation necrosis in the posterior cranial fossa: technical note, *Neurosurgical Focus FOC*, *41*(4), E5. Retrieved Aug 13, 2021, from https://thejns.org/focus/view/journals/neurosurg-focus/41/4/article-pE5.xml

[12] Dowlatshahi K, Francescatti DS, Bloom KJ. Laser therapy for small breast cancers. Am J Surg. 2002 Oct;184(4):359-63. doi: 10.1016/s0002-9610(02)00942-x. PMID: 12383903.

[13]O. Bonhomme, B. Duysinx, V. Heinen, N. Detrembleur, J.-L. Corhay, R. Louis. First report of probe based confocal laser endomicroscopy during medical thoracoscopy, Respiratory Medicine, Volume 147, 2019

[14] Fugazza, Alessandro et al. "Confocal Laser Endomicroscopy in Gastrointestinal and Pancreatobiliary Diseases: A Systematic Review and Meta-Analysis." BioMed research international vol. 2016 (2016): 4638683. doi:10.1155/2016/4638683

[15] Strunk CL, Nichols ML. A comparison of the KTP/532-laser tonsillectomy vs. traditional dissection/snare tonsillectomy. Otolaryngol Head Neck Surg. 1990 Dec;103(6):966-71. doi: 10.1177/019459989010300614. PMID: 2126131.

[16]Ishlah LW, Fahmi AM, Srinovianti N. Laser versus dissection technique of tonsillectomy. Med J Malaysia. 2005 Mar;60(1):76-80. PMID: 16250284.

[17]Nagel, Suzanne R., and Thomas G. Brown. "Optical Fibers." AccessScience, McGraw-Hill Education, Jan. 2020.

[18]High-Performance Beam Collimators. (2021). Science (American Association for the Advancement of Science), 372(6546), 1113–.

[19] R. Paschotta, article on 'fiber collimators' in the RP Photonics Encyclopedia, accessed on 2021-08-13

[20] *Insights into Collimating Light from Different Types of Light Sources*. THORLABS. (2021, April 20). https://www.thorlabs.com/newgrouppage9.cfm?objectgroup_id=12211.

[21]Sotor, J. Z., Antończak, A. J., & Abramski, K. M. (2010). Single-longitudinal mode Nd:YVO4/YVO4/KTP green solid state laser. Opto-Electronics Review, 18(1), 75–79. https://doi.org/10.2478/s11772-009-0028-5

[22]Li, C., Huang, J., Wang, K., Liu, Q., & Chen, Z. (2020). Investigation on thermal damage model of skin tissue in vitro by infrared laser welding. Optics and Lasers in Engineering, 124, 105807. https://doi.org/10.1016/j.optlaseng.2019.105807

[23]Huusmann, S., Wolters, M., Kramer, M. W., Bach, T., Teichmann, H., Eing, A., Bardosi, S., & Herrmann, T. R. W. (2016). Tissue damage by laser radiation: An in vitro comparison between Tm:YAG and Ho:YAG laser on a porcine kidney model. SpringerPlus, 5(1), 1–8. SciTech Premium Collection. https://doi.org/10.1186/s40064-016-1750-3

[24]Kirschbaum, A., Braun, S., Rexin, P., Bartsch, D. K., & Seyfer, P. (2014). Comparison of local tissue damage: Monopolar cutter versus Nd:YAG laser for lung parenchyma resection. An experimental study. Interactive CardioVascular and Thoracic Surgery, 18(1), 1–6. https://doi.org/10.1093/icvts/ivt419

[25]Bown, S. G. (1998). Science, medicine, and the future. New techniques in laser therapy. BMJ (Clinical Research Ed.), 316(7133), 754–757. PubMed. https://doi.org/10.1136/bmj.316.7133.754

[26]Kwiatkowski, S., Knap, B., Przystupski, D., Saczko, J., Kędzierska, E., Knap-Czop, K., Kotlińska, J., Michel, O., Kotowski, K., & Kulbacka, J. (2018). Photodynamic therapy – mechanisms, photosensitizers and combinations. Biomedicine & Pharmacotherapy, 106, 1098–1107.

[27]Pearce, J. (2011). Mathematical models of laser-induced tissue thermal damage. International Journal of Hyperthermia, 27(8), 741–750. https://doi.org/10.3109/02656736.2011.580822

[28]The Fiber Optic Association, Inc. (2018). *Optical Fiber*. The FOA reference for fiber optics - optical fiber. https://www.thefoa.org/tech/ref/basic/fiber.html.

[29]*0.39 NA TECS-Clad Multimode Optical Fiber, Step Index*. THORLABS. (2021, April 20). https://www.thorlabs.com/newgrouppage9.cfm?objectgroup_id=6845&pn=FT200UMT#5652

[30]Wilmink, G., Opalenik, S., Beckham, J., Davidson, J., & Jansen, E. (2006). Assessing laser-tissue damage with bioluminescent imaging. Journal of Biomedical Optics, 11, 041114. https://doi.org/10.1117/1.2339012

[31]Zhang, H., Liu, K., Xue, Z., Yin, H., Dong, H., Jin, W., Shi, X., Wang, H., & Wang, H. (2018). High-voltage pulsed electric field plus photodynamic therapy kills breast cancer cells by triggering apoptosis. American Journal of Translational Research, 10(2), 334–351. PubMed.

[32] Norris JL, Caprioli RM. Analysis of tissue specimens by matrix-assisted laser desorption/ionization imaging mass spectrometry in biological and clinical research. *Chem Rev*. 2013;113(4):2309-2342. doi:10.1021/cr3004295

[33]Evangelista, L., De Meo, B., Bernabei, G., Belloni, G., D'Angelo, G., Vanzini, M., Calzà, L., & Gallamini, M. (2019). Ultra-Low-Level Laser Therapy and Acupuncture Libralux: What Is so Special?. Medicines (Basel, Switzerland), 6(1), 40. https://doi.org/10.3390/medicines6010040

[34]Giuliani, A., Lorenzini, L., Gallamini, M., Massella, A., Giardino, L., & Calzà, L. (2009). Low infrared laser light irradiation on cultured neural cells: effects on mitochondria and cell viability after oxidative stress. BMC complementary and alternative medicine, 9, 8. https://doi.org/10.1186/1472-6882-9-8

[35] Cummings BS, Schnellmann RG. Measurement of cell death in mammalian cells. *Curr Protoc Pharmacol*. 2004;Chapter 12:10.1002/0471141755.ph1208s25. doi:10.1002/0471141755.ph1208s25

[36]Fichera L. (2016) Conclusions and Future Research Directions. In: Cognitive Supervision for Robot-Assisted Minimally Invasive Laser Surgery. Springer Theses (Recognizing Outstanding Ph.D. Research). Springer, Cham. https://doi.org/10.1007/978-3-319-30330-7_7

[37] O'Connor, J., Akbar, F. B., Hutson, M. S., & Page-McCaw, A. (2021, September 27). *Zones of cellular damage around pulsed-laser wounds*. PLOS ONE. Retrieved January 30, 2022, from https://journals.plos.org/plosone/article?id=10.1371%2Fjournal.pone.0253032

[38] Yan, Y., Olszewski, A. E., Hoffman, M. R., Zhuang, P., Ford, C. N., Dailey, S. H., & Jiang, J. J. (2010). Use of lasers in laryngeal surgery. *Journal of voice : official journal of the Voice Foundation*, 24(1), 102–109. https://doi.org/10.1016/j.jvoice.2008.09.006

[39] Kroemer, G., Galluzzi, L., Vandenabeele, P., Abrams, J., Alnemri, E. S., Baehrecke, E. H., Blagosklonny, M. V., El-Deiry, W. S., Golstein, P., Green, D. R., Hengartner, M., Knight, R. A., Kumar, S., Lipton, S. A., Malorni, W., Nuñez, G., Peter, M. E., Tschopp, J., Yuan, J., Piacentini, M., … Nomenclature Committee on Cell Death 2009 (2009). Classification of cell death: recommendations of the Nomenclature Committee on Cell Death 2009. Cell death and differentiation, 16(1), 3–11. https://doi.org/10.1038/cdd.2008.150